Article

Cell Reports

Nidogen-1 Contributes to the Interaction Network Involved in Pro-B Cell Retention in the Peri-sinusoidal Hematopoietic Stem Cell Niche

Graphical Abstract

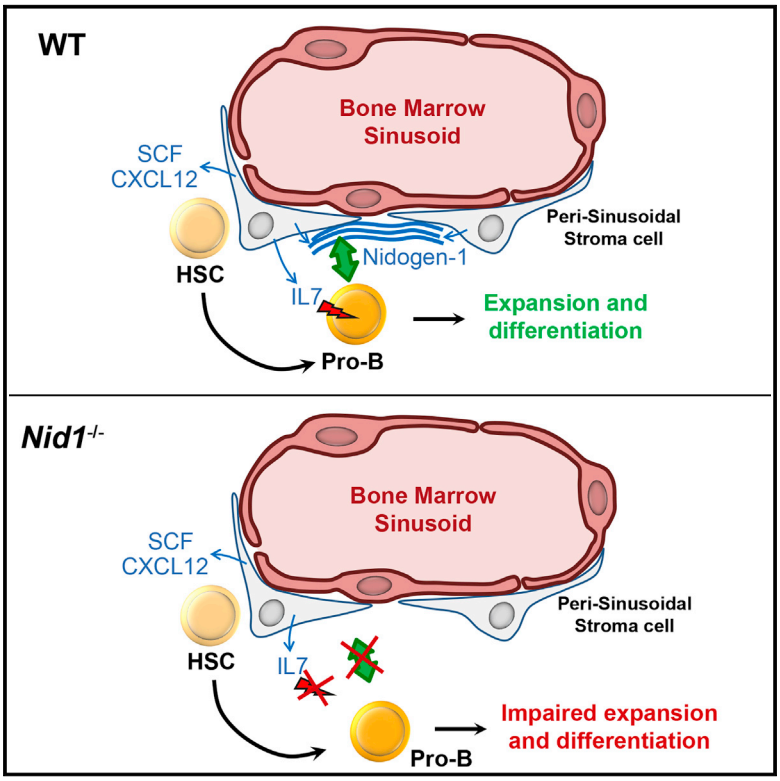

Highlights

- Murine peri-sinusoidal stromal cells co-express HSC and early B cell niche genes
- HSCs and early B cells form specific interaction networks with PSS cells
- Nidogen-1 is involved in pro-B cell retention in the peri-sinusoidal niche
- Stromal cells with similar characteristics are present in human bone marrow

Authors

Marielle Balzano, Maria De Grandis, Thien-Phong Vu Manh, ..., Michel Aurrand-Lions, Claudine Schiff, Stéphane J.C. Mancini

Correspondence

michel.aurrand-lions@inserm.fr (M.A.-L.), stephane.mancini@inserm.fr (S.J.C.M.)

In Brief

Balzano et al. show that bone marrow peri-sinusoidal stromal cells, which form the hematopoietic stem cell niche, also express B cell niche genes including IL-7 and Nidogen-1. Loss of Nidogen-1 expression specifically affects access of pro-B cells to IL-7, resulting in impaired expansion and differentiation of early B cells.

Balzano et al., 2019, Cell Reports *26*, 3257–3271
March 19, 2019
https://doi.org/10.1016/j.celrep.2019.02.065

CellPress

Cell Reports
Article

Nidogen-1 Contributes to the Interaction Network Involved in Pro-B Cell Retention in the Peri-sinusoidal Hematopoietic Stem Cell Niche

Marielle Balzano,[1,2] Maria De Grandis,[1] Thien-Phong Vu Manh,[2] Lionel Chasson,[2] Florence Bardin,[1] Anne Farina,[3,4] Arnauld Sergé,[1] Ghislain Bidaut,[1] Pierre Charbord,[5] Léonard Hérault,[1,6] Anne-Laure Bailly,[1] Amandine Cartier-Michaud,[1] Annie Boned,[2] Marc Dalod,[2] Estelle Duprez,[1] Paul Genever,[7] Mark Coles,[8] Marc Bajenoff,[2] Luc Xerri,[9] Michel Aurrand-Lions,[1,10,*] Claudine Schiff,[2,10] and Stéphane J.C. Mancini[1,2,11,*]

[1]Aix-Marseille University, CNRS, INSERM, Institut Paoli-Calmettes, CRCM, Marseille, France
[2]Aix-Marseille University, CNRS, INSERM, CIML, Marseille, France
[3]ICEP Platform, Aix-Marseille University, CNRS, INSERM, Institut Paoli-Calmettes, CRCM, Marseille, France
[4]MI-Mabs, Aix-Marseille University, Marseille, France
[5]Sorbonne Université, Institut de Biology Paris-Seine, Laboratoire de Biologie du Développement, Paris, France
[6]Aix-Marseille University, CNRS, Centrale Marseille, I2M, Marseille, France
[7]Department of Biology, University of York, York YO10 5DD, UK
[8]Kennedy Institute of Rheumatology, University of Oxford, Oxford, OX3 7FY, UK
[9]Department of Bio-Pathology, Institut Paoli-Calmettes, Aix-Marseille University, Marseille, France
[10]Senior author
[11]Lead Contact
*Correspondence: michel.aurrand-lions@inserm.fr (M.A.-L.), stephane.mancini@inserm.fr (S.J.C.M.)
https://doi.org/10.1016/j.celrep.2019.02.065

SUMMARY

In the bone marrow, CXCL12 and IL-7 are essential for B cell differentiation, whereas hematopoietic stem cell (HSC) maintenance requires SCF and CXCL12. Peri-sinusoidal stromal (PSS) cells are the main source of IL-7, but their characterization as a pro-B cell niche remains limited. Here, we characterize pro-B cell supporting stromal cells and decipher the interaction network allowing pro-B cell retention. Preferential contacts are found between pro-B cells and PSS cells, which homogeneously express HSC and B cell niche genes. Furthermore, pro-B cells are frequently located in the vicinity of HSCs in the same niche. Using an interactome bioinformatics pipeline, we identify Nidogen-1 as essential for pro-B cell retention in the peri-sinusoidal niche as confirmed in Nidogen-1$^{-/-}$ mice. Finally, human pro-B cells and hematopoietic progenitors are observed close to similar IL-7^{+} stromal cells. Thus, a multispecific niche exists in mouse and human supporting both early progenitors and committed hematopoietic lineages.

INTRODUCTION

The influence of bone marrow (BM) mesenchymal stromal cells on the differentiation program of mouse hematopoietic cells has become increasingly clear over the last few years. A number of stromal cell niches have been described, not only for hematopoietic stem cells (HSCs) but also for B cell progenitors (Aurrand-Lions and Mancini, 2018). Stromal cells supporting HSC maintenance have been separated into perivascular and endosteal/peri-arteriolar niches. Indeed, recent results indicate that HSC maintenance relies on peri-sinusoidal stromal (PSS) cells, which secrete CXCL12 and stem cell factor (SCF) (Ding and Morrison, 2013; Ding et al., 2012; Méndez-Ferrer et al., 2010; Sugiyama et al., 2006), while arteriole-associated pericytes expressing Nestin have been shown to control HSC quiescence (Kunisaki et al., 2013). Furthermore, arteriolar cells close to the bone surface as well as sinusoidal BM endothelial cells (sBMECs) also contribute to HSC maintenance and retention in the BM (Ding and Morrison, 2013; Ding et al., 2012; Itkin et al., 2016). After commitment to the B cell lineage, progenitor development depends on CXCL12 and interleukin-7 (IL-7). Mice deficient for CXCL12 or CXCR4 present B cell differentiation and retention defects that start at the earliest pre-pro-B cell stages (Egawa et al., 2001; Ma et al., 1998, 1999). IL-7 controls the commitment of lymphoid progenitors to the B cell lineage and is required for pro-B and pre-B cell proliferation (Dias et al., 2005; Marshall et al., 1998).

In support of these results, pre-pro-B cells have been localized near BM stromal cells expressing CXCL12, before re-localization in the vicinity of IL-7-expressing stromal cells at the pro-B cell stage (Tokoyoda et al., 2004). Most of the stromal cells expressing CXCL12 or IL-7 were localized in peri-sinusoidal areas of the BM (Mourcin et al., 2011; Sugiyama et al., 2006). However, other studies have suggested that osteoblasts (OBs) play a central role in early B cell development (Wu et al., 2008; Zhu et al., 2007). Finally, IL-7 depletion from CD31^{+} BM endothelial cells (BMECs) causes a drop in B cell numbers (Cordeiro Gomes et al., 2016), suggesting that endothelial sources of IL-7 are required for B cell differentiation. More recently, it has been demonstrated that the large majority of pro-B and pre-B cells are located in

the same niche, but are respectively static and motile (Fistonich et al., 2018). This has been attributed to cross-circuitry between IL-7R and pre-BCR signaling, which positively and negatively control $\alpha4\beta1$ integrin-mediated adhesion, suggesting that high level of IL-7R signaling in sessile pro-B cells is due to increased exposure to IL-7 while pre-BCR signaling turns the motility on.

The heterogeneity of BM stromal cell niches remains unclear because of the use of multiple reporter mice strains and experimental setups. The study of CXCL12-GFP and SCF-GFP knockin mice revealed that PSS cells are the main source of CXCL12 and SCF (Ding et al., 2012; Omatsu et al., 2010; Sugiyama et al., 2006). Co-expression of these factors by LepR$^+$ PSS cells has been confirmed using CXCL12-dsRed/SCF-GFP double-knockin mice (Ding and Morrison, 2013). With regard to early B cell niches, it was initially postulated that distinct stromal cell subpopulations express CXCL12 and IL-7 (Tokoyoda et al., 2004). However, we identified a BM stromal cell subpopulation co-expressing these two factors (Mourcin et al., 2011). This population was phenotypically defined as CD45$^-$CD54$^+$CD31$^-$BP1$^+$ stromal cells and morphologically similar to LepR$^+$ cells that co-express CXCL12 and SCF (Ding et al., 2012), suggesting that LepR$^+$ cell may co-express IL-7, SCF, and CXCL12. In accordance with these findings, a recent study showed that some LepR$^+$ stromal cells co-express IL-7, SCF, and CXCL12 (Cordeiro Gomes et al., 2016). Importantly, specific deletion of CXCL12 using LepR-Cre/Cxcl12$^{lox/lox}$ mice has a more profound effect on HSC maintenance than deletion using IL-7-Cre/Cxcl12$^{lox/lox}$ mice, suggesting that several PSS subsets specialized in HSC maintenance or IL-7 secretion may exist.

In the current study, we phenotypically characterized BM stromal cell niches that were previously identified based on reporter gene expression. This analysis revealed a limited diversity of BM mesenchymal subsets, and PSS cells were found to co-express LepR, BP1, CXCL12, SCF, and IL-7 at the single-cell level. HSCs and pro-B cells were often simultaneously associated to PSS cells and respectively formed specific interaction networks involving genes implicated in HSC maintenance and lymphoid development. Furthermore, among factors expressed by PSS cells, we identified Nidogen-1 as a specific retention signal for pro-B cells in the peri-sinusoidal niche. Finally, a global gene expression analysis revealed that murine PSS cells were identical to CD317$^+$ human BM stromal cells, and that both hematopoietic stem and progenitor cells (HSPCs) and pro-B cells were located close to these cells. Taken together, our results demonstrate the existence of a homogeneous BM stromal cell population present in mouse and human that has the capacity to produce niche factors involved in the maintenance and development of distinct hematopoietic subsets.

RESULTS

Mesenchymal Cell Characterization in BM Reveals the Existence of a Restricted Number of Subsets

To define mesenchymal cell heterogeneity in the BM, we used multiparametric flow cytometry to simultaneously analyze the different phenotypic markers described separately in the literature. BM cells were separated into conduit or bone fractions. In the conduit fraction, CD31$^+$ BMECs were mainly composed of Sca1^{lo}Endomucin (Emcn)^{lo} L-type sBMECs and of low numbers of Sca1$^+$Emcn$^-$ arteriolar BMECs (aBMECs) as expected (Kusumbe et al., 2014). Two CD51$^+$ stromal subsets were identified (Figures 1A and 1B). CD54^{lo}NG2$^+$ cells corresponded to pericytes and CD54$^+$NG2$^-$ stromal cells expressed high levels of LepR, indicating that they were PSS cells. Furthermore, PSS cells expressed CD106, marker of CAR cells (Tokoyoda et al., 2004), as well as BP1 and CD317, markers of IL-7$^+$ PSS cells (James et al., 2015; Mourcin et al., 2011), suggesting that they may correspond to a single subset. In contrast, the bone fraction was enriched for aBMECs, H-type (Sca1$^+$Emcn^{hi}) BMECs, few L-type sBMECs, and CD51$^+$ mesenchymal cells (Figure 1C). Few PSS cells were observed and CD51$^+$CD54$^{lo/-}$BP1$^-$ cells mostly corresponded to OBs as they did not express the immature mesenchymal cell marker CD105 but expressed high levels of *Bglap*, *Col1a1*, *Col2a1* genes specific for mature OBs (Figure 1D). These results suggest that BM mesenchymal subsets are essentially composed of MSCs, PSS cells, pericytes, and OBs.

Pro-B Cells Are in Direct Contact with PSS Cells

We next explored the localization of pro-B cells with respect to PSS cells. LepR$^+$ cells were clearly identified in the vicinity of sinusoidal structures (Figure 1E). In the BM, most terminal deoxynucleotidyl transferase (TdT)-positive cells corresponded to pro-B cells (Figures 1E and S1). TdT$^+$ cells were detected close to LepR$^+$ PSS cells and mainly away from the endosteum (Figure 1F). Furthermore, localization of pro-B cells close to LepR$^+$ cells was specific since cells positioned randomly in the same images were found to be at a significantly greater distance, whereas their positioning relative to the bone was not different. These results indicate that PSS cells form a cellular niche for pro-B cells.

IL-7 Is Exclusively Expressed by PSS Cells Co-expressing High Levels of CXCL12 and SCF

Previous results showed that PSS cells are composed of IL-7$^+$ and IL-7$^-$ subsets (Cordeiro Gomes et al., 2016). In order to analyze these subsets molecularly and their relation to pro-B cells, we used IL-7-Cre/Rosa-eYFP mice (hereafter IL-7 reporter mice). YFP expression was only detected in PSS cells, pericytes, and OBs (Figures 2A and 2B), and YFP$^+$ BMECs were neither detected in the conduit nor in the bone fraction (n = 10). As shown earlier (Cordeiro Gomes et al., 2016; Mourcin et al., 2011), most of the YFP$^+$ cells in adult mice corresponded to PSS cells (Figures 2A, S2A, and S2B). Furthermore, most of the LepR$^+$ PSS cells were YFP$^+$ in contrast to pericytes and OBs (Figure 2C).

YFP$^+$ stromal cells were next isolated from the conduit and bone fractions from IL-7 reporter mice, and tested for gene expression by qPCR. *Il7* was expressed by PSS cells sorted from both fractions but was not detected in pericytes or OBs, regardless of YFP expression status (Figure 2D). Since YFP expression is irreversible in the Rosa-eYFP system once the Cre recombinase has been expressed, this result indicates that YFP expression may be related to lineage tracing of a progenitor cell expressing IL-7. This is the case for OBs, which are known to be generated from PSS cells in adult mice but not in young animals (Mizoguchi et al., 2014). Indeed, in contrast to adult, none of

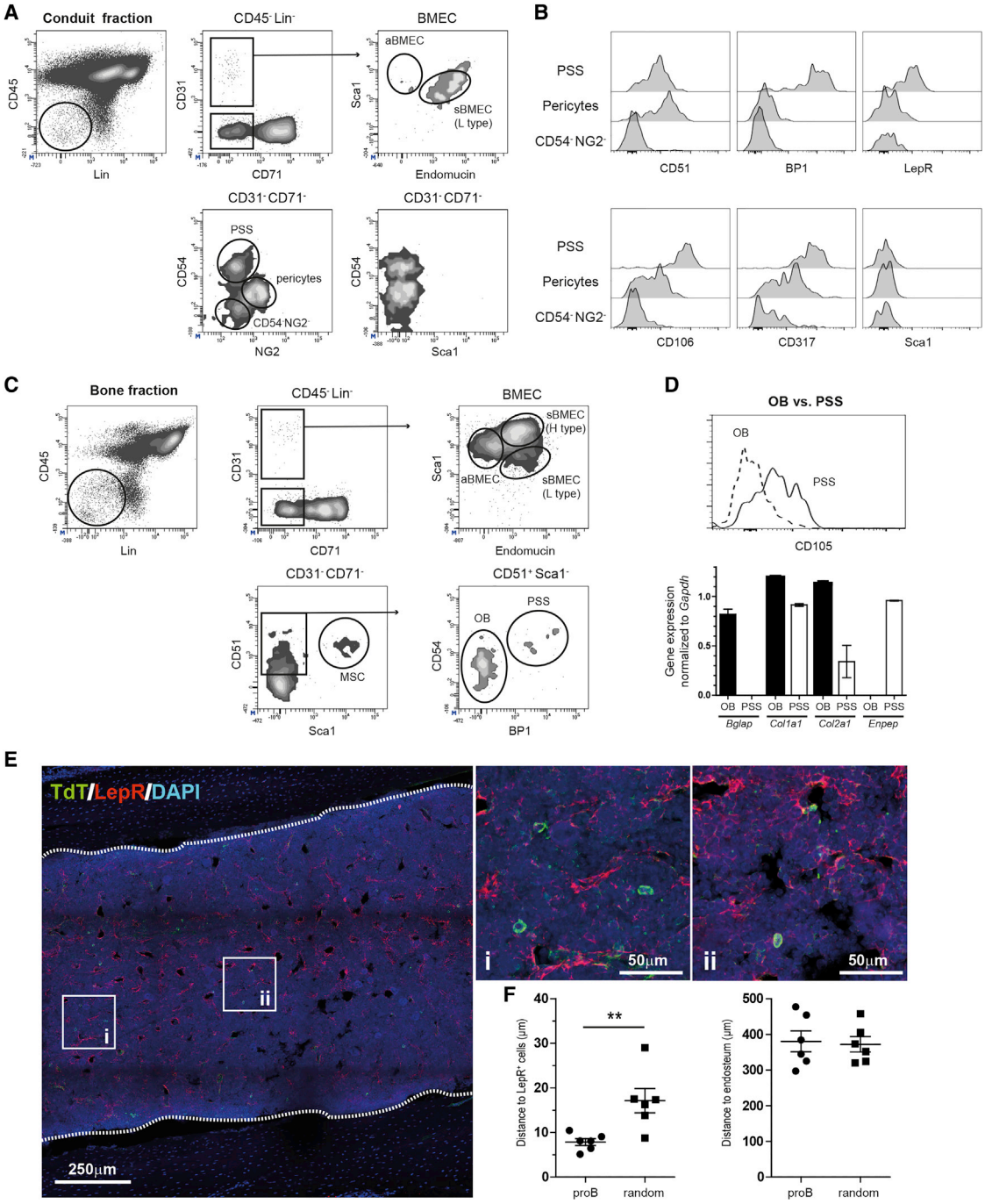

Figure 1. Phenotypic Characterization of the BM Microenvironment and Pro-B Cell Localization

(A) Analysis of the conduit fraction by flow cytometry. The dot plots show the strategy used to identify BMECs, PSS cells, and pericytes.

(B) Phenotypic characterization of the stromal cell subsets gated on the subpopulations shown in (A).

(C) Analysis of the bone fraction by flow cytometry. The dot plots show the strategy used to identify BMECs, MSCs, OBs, and PSS cells.

(D) CD105 expression by $CD51^{+}Sca1^{-}CD54^{lo/-}BP1^{-}$ compared to PSS cells by flow cytometry (top) and qPCR analysis of the indicated genes (bottom).

(E) Immunostaining of pro-B (TdT^{+}; see also Figure S1) and PSS cells (stained with an anti-LepR antibody) on BM sections of C57BL/6J mice. Two representative regions were magnified. The images were obtained from maximum-intensity projection of tile Z scans. The bone border is represented as a dotted line.

(F) The 3D distance between pro-B and $LepR^{+}$ PSS cells (left) and between pro-B and the bone surface (right) is shown as the average distance per mouse (n = 6; 191 TdT^{+} cells in total) and is compared to the distance measured after *in silico* random positioning of pro-B cells. The distances were measured on 3D images as shown in (E). Error bars represent the SEM. Statistical significance was calculated using an unpaired t test. $^{**}p < 0.01$.

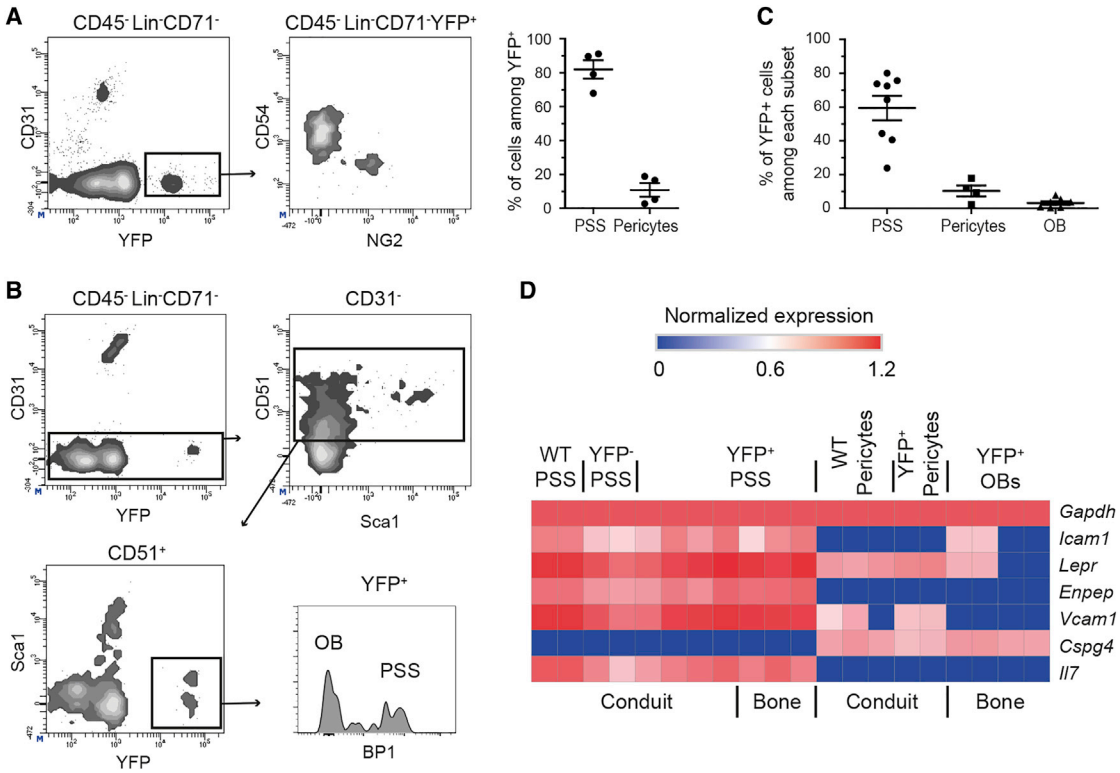

Figure 2. PSS Cells Are the Major Source of IL-7 in the BM

(A) Stromal cells from the conduit fraction of IL-7 reporter mice were gated on the YFP$^+$ population and further analyzed based on expression of CD54 and NG2 (n = 4 mice).

(B) Analysis by flow cytometry of mesenchymal cells from the bone fraction showing the YFP$^+$ subsets (PSS cells, n = 8 mice; pericytes, n = 4; OBs, n = 7).

(C) Proportion of YFP$^+$ cells among PSS, pericytes, and OBs determined by flow cytometry. Error bars in (B) and (C) indicate SEM.

(D) qPCR was performed on sorted PSS cells and pericytes from WT mice, and on PSS cells, pericytes, and OBs from IL-7 reporter mice after gating on YFP$^+$ cells. YFP$^-$ PSS cells were also sorted. For each gene, the expression level was normalized relative to *Gapdh* before representing levels on a heatmap. High expression is indicated in red, and low expression in blue. See also Figure S2.

the bone lining cells in 2- to 3-week-old IL-7 reporter expressed YFP (Figures S2A–S2C).

Since YFP$^+$ PSS cells represented only 59.4% of total PSS cells (Figure 2C), their gene expression signature was compared to PSS cells contributing to the HSC niche. Gene expression profiles obtained from PSS cells isolated from wild-type (WT) mice as well as YFP$^+$ and YFP$^-$ PSS cells from IL-7 reporter mice were compared to public datasets of PSS sorted from CXCL12-GFP$^+$, CXCL12-dsRed$^+$, Nestin-GFP^{lo}, and SCF-GFP$^+$ stromal cells. Microarrays from total BM were used as a reference control between datasets and gene expression profiles for BMECs, OBs, and MSCs as unrelated datasets. Unsupervised principal-component analysis (PCA) showed that the stromal cell subpopulations independently sorted from CXCL12, SCF, Nestin, and IL-7 reporter mice clustered together (Figure 3A), and were distant from BMECs, OBs, and MSCs. Technical bias most probably account for the spreading of the PSS cluster along the first dimension. Indeed, SCF-GFP$^+$ cells as well as total BM samples from the same dataset were distant to a similar extent from our PSS cell and total BM samples, respectively. Furthermore, spreading was also observed for PSS cells sorted from two different CXCL12 reporter mouse models using GFP and dsRed, respectively (Decker et al., 2017; Greenbaum et al., 2013). Interestingly, PSS cells isolated from WT mice were identical to YFP$^-$ PSS cells from IL-7 reporter mice and both populations clustered with the other PSS cell datasets, indicating that Cre/lox recombination is only partial in IL-7 reporter mice, and that PSS cells may represent a homogeneous population. This result was confirmed by qPCR showing *Il7* expression in YFP$^-$ PSS cells (Figure 2D). Unsupervised hierarchical clustering revealed that the PSS cells from the different datasets expressed both HSC and B cell niche genes (Figure 3B). Notably, *Il7*, *Cxcl12*, and *Kitl* (encoding SCF) were co-expressed in PSS cells irrespective of dataset origin and of the reporter system used, and this result was confirmed by single-cell qPCR analysis on PSS cells isolated from WT mice and compared to pericytes (Figure 3C). Finally, single-cell RNA sequencing (scRNA-seq) of BM stromal cells showed that PSS cells formed a single cluster based on the significant upregulation and downregulation of 443 and 371 genes, respectively, as compared to MSCs, OBs, BMECs, or pericytes (Figures 3D and S3; Table S1). Altogether, these results indicate that *Il7*, *Cxcl12*, and *Kitl* are co-expressed by CD54$^+$BP1$^+$ PSS cells, and that these cells are identical to peri-sinusoidal CAR, Nestin-GFP^{lo}, and SCF$^+$LepR$^+$ cells.

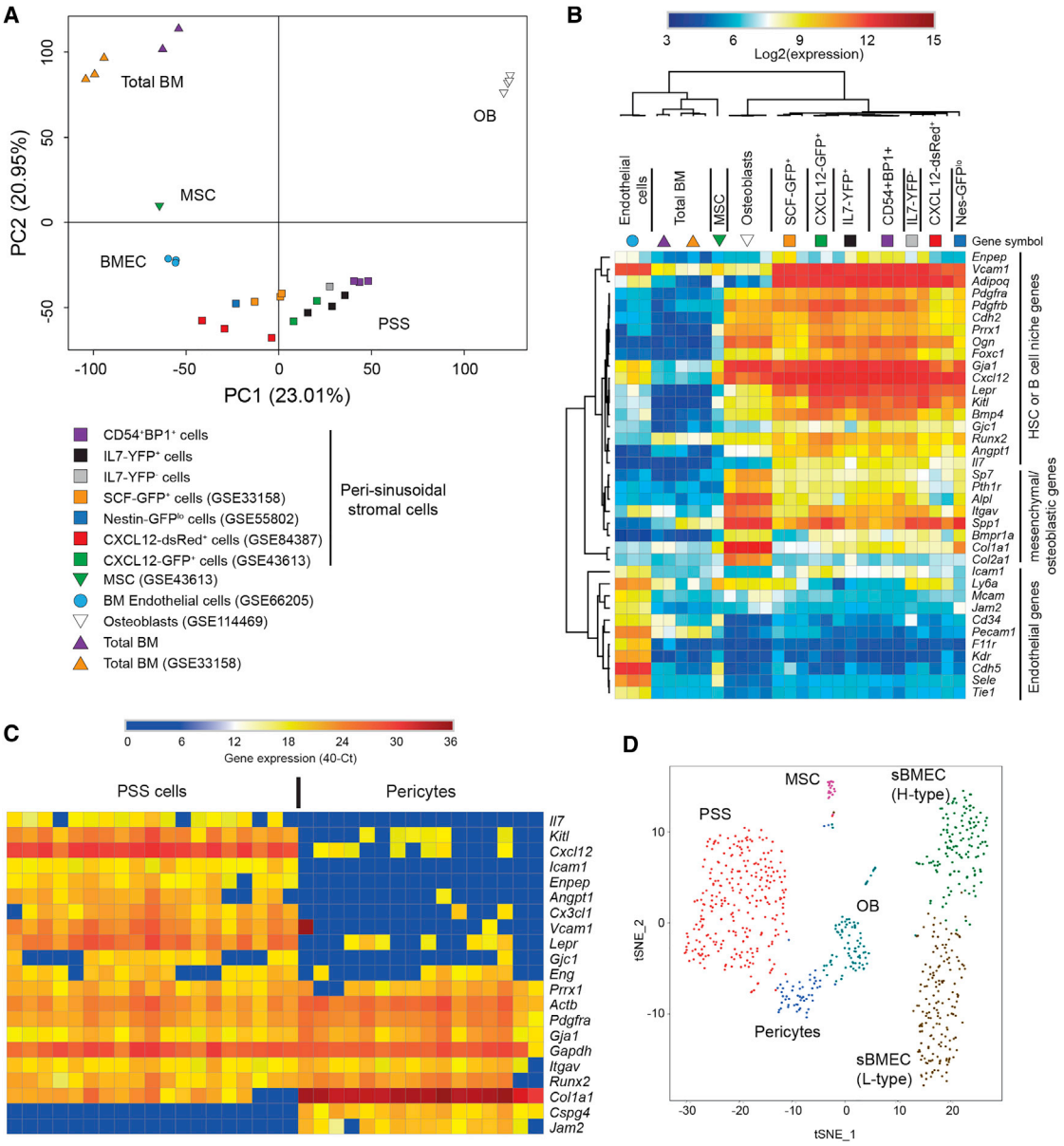

Figure 3. IL-7, CXCL12, and SCF Are Co-expressed by the PSS Cell Subset

(A) The relationships between the different subpopulations indicated were determined by PCA. Numbers between brackets along axes indicate the proportion of variance represented by PC1 and PC2.

(B) Heatmap of selected endothelial, mesenchymal/osteoblastic, and "niche genes" using datasets shown in (A). Unsupervised clustering was performed for each row and column.

(C) Heatmap showing unsupervised clustering of single-cell gene expression by PSS cells and pericytes. Single cells are shown in columns and genes in rows.

(D) t-distributed stochastic neighbor embedding (t-SNE) analysis of mesenchymal and endothelial cells sorted from the BM of C57BL/6J mice and subjected to scRNA-seq. Genes representative of each subset were used to define the identity of the clusters (see Figure S3). Number of cells: PSS cells, n = 271; L-type BMECs, n = 163; H-type BMECs, n = 137; OBs, n = 86; pericytes, n = 54; MSCs, n = 18. The t-SNE analysis is representative of two independent experiments.

PSS Cells Simultaneously Accommodate HSCs and Early B Cells, Forming Specific Interaction Networks with Them

We next examined the relative localization of HSCs and pro-B cells with respect to PSS cells. HSCs were defined as Lineage-negative (Lin$^-$)CD41$^-$CD48$^-$ cells expressing CD150 (Ding and Morrison, 2013; Kunisaki et al., 2013) and pro-B cells as TdT$^+$ cells. Both cell subsets were located close to LepR$^+$ PSS cells and were frequently seen in contact with the same LepR$^+$ stromal cell (Figure 4A; Video S1). Furthermore, the distribution analysis for HSCs compared to their closest pro-B cell neighbors in three dimensions (3D) revealed that 15.2% were at a distance

of less than 16 μm (two-cell distance) and 50% at less than 41.7 μm (five-cell distance) (Figure 4B). Simulations of pro-B cell random positioning in the image produced a significantly greater average distance between pro-B cells and HSCs. These results demonstrate that HSCs and pro-B cells are in the vicinity of PSS cells and that migration of pro-B cell differentiating from HSCs occurs over a relatively restricted area.

Since PSS cells have the capacity to sustain the development of both HSCs and pro-B cells, we looked for receptor/ligand pairs that could explain such multispecific cognate interactions. To do so, we defined the interactome between PSS cells and long-term (LT)-HSCs or pro-B cells. Pre-pro-B cells have been reported to be in contact with PSS cells (Tokoyoda et al., 2004) and were therefore used as positive controls. As negative controls, we used the closest related hematopoietic subsets localized to distinct niches: short-term (ST)-HSCs or pre-B cells (Kiel et al., 2005; Mourcin et al., 2011) (Figure 4C). An interactome bioinformatics pipeline was developed to confront gene expression datasets from YFP$^+$ PSS cells from IL-7 reporter mice and publicly available datasets for LT-HSCs, ST-HSCs, pre-pro-B cells, pro-B cells, and pre-B cells. Genes encoding for trans-interacting ligand/receptor pairs were identified (Table S2). When comparing LT-HSCs to ST-HSCs, a higher number of gene products expressed by LT-HSCs were found to interact with gene products expressed by PSS cells (12 gene products specifically expressed by LT-HSCs had a ligand expressed by PSS cells compared to 1 for ST-HSCs; Figure 4D). Similarly, higher numbers of genes specifically expressed in pre-pro-B and pro-B cells were involved in interactions with PSS cells compared to pre-B cells. Furthermore, LT-HSC, pre-pro-B cell, or pro-B cell-specific genes involved in interactions with PSS cells—as identified in Figure 4D—were highly relevant niche genes, as demonstrated by the greater significant enrichment for Gene Ontology (GO) terms related to adhesion, secretion, differentiation, or proliferation compared to ST-HSCs or pre-B cells, respectively (Figure 4E; Table S3). We next compared the expression signatures of LT-HSCs, pre-pro-B cells, and pro-B cells by focusing on genes implicated in interaction with PSS cells. As expected, *Cxcr4*, *Kit*, and the *Il7r*/*Il2rg* heterodimer were identified as hematopoietic genes encoding ligands for CXCL12, SCF, and IL-7, respectively (Figure 4F). More than 50% of the genes identified encoded proteins with known functions in HSPC maintenance or lymphoid development and migration. Among these, we found ligand/receptor pairs that have been extensively studied in HSC regulation (Tie2/Angiopoietin-1, TGFβR/TGFβ, Integrinα6β1/Laminin) or in early B cell development (α4β1/VCAM-1). Furthermore, although some overlapping gene expression was found between LT-HSCs and pre-pro-B or pre-pro-B and pro-B cells, there were few overlaps between LT-HSCs and pro-B cells. Finally, we found that hematopoietic cells expressed growth factors involved in the development of mesenchymal or endothelial cells, indicating that reciprocal interactions between PSS and hematopoietic cells contribute to the maintenance of hematopoietic niches.

We then tested whether genes encoding niche proteins involved in hematopoietic/PSS cell interactions were also expressed by sBMECs or ALCAM$^+$Sca1$^-$ and ALCAM$^-$Sca1$^-$ OBs (Nakamura et al., 2010). Gene set enrichment analysis (GSEA) revealed a significant enrichment (false discovery rate [FDR] < 0.25) for niche gene expression by PSS cells as compared to sBMECs and ALCAM$^+$Sca1$^-$ or ALCAM$^-$Sca1$^-$ OBs (Figure 4G). Moreover, unsupervised hierarchical clustering performed on HSC and B cell niche genes identified earlier confirmed that the highest levels of these genes, including *Cxcl12*, *Kitl*, and *Il7*, were found in PSS cells (Figure S4). These results show that LT-HSCs, pre-pro-B cells, and pro-B cells express a network of genes allowing preferential interactions with PSS cells rather than endothelial or osteoblastic cells.

Nidogen-1 Is Implicated in Pro-B Cell Retention in Their Niche

Among the genes involved in the specific interaction between PSS cells and pro-B cells, we identified the ligand/receptor pair *Nid1*/*Plxdc1*. Nidogen-1 is part of the basement membrane together with laminin and is involved in matrix to cell interactions with PLXDC1 expressed at the plasma membrane (Lee et al., 2006). *Plxdc1* expression was shown to be controlled by the B cell transcription factor Pax5 (Revilla-I-Domingo et al., 2012). Pro-B cells indeed expressed PLXDC1 and were located close to LepR$^+$Nid1$^+$ sinusoidal structures (Figure 5A). Importantly, expression of CD51, another cellular ligand for Nidogen-1 (Yi et al., 1998), was undetectable in pro-B cells (Figure S5A), suggesting that pro-B cell interaction with Nidogen-1 depends on PLXDC1. The influence of Nidogen-1 deficiency on pro-B cell differentiation was analyzed in *Nid1*$^{-/-}$ mice. Total BM cellularity and B cell frequencies were normal in *Nid1*$^{-/-}$ mice (Figures 5B and S5B). However, the frequency of pre-BI cells was specifically decreased, revealing impaired pro-B to pre-BI cell transition. The decrease in pre-BI cells in *Nid1*$^{-/-}$ mice had repercussions on the proportion of the later large pre-BII cells, and thus on the most immature BP1$^+$ pre-BII cells, even though the overall frequency of pre-BII cells was not affected (Figures 5B and S5B). As a consequence, immature and recirculating B cells were also normally represented. This result indicates that the defect observed in *Nid1*$^{-/-}$ mice is transient, and specific to the pro-B to pre-BI cell transition. In pre-BII cells, the pre-BCR induces a strong proliferation, which may explain the recovery in *Nid1*$^{-/-}$ mice. We thus analyzed *de novo* B cell differentiation in WT and *Nid1* deficient mice 7 days after injection of the cytostatic agent hydroxyurea (HU) as described previously (Espeli et al., 2009). Pre-pro-B cells were not affected, but the frequency of B cells was significantly decreased from the pro-B/pre-BI cell transition to the following differentiation subsets, confirming the existence of homeostatic compensation at the pre-BII stage at steady state (Figure S5B).

To determine whether this bottleneck is due to reduced accessibility to IL-7, we checked IL-7 receptor signaling-mediated phosphorylation of STAT5 and early B cell proliferation. As expected, phospho-STAT5 (pSTAT5) levels and the proportion of proliferating cells were significantly higher in pro-B compared to pre-BI cells in WT animals (Figures 5C, 5D, S5D, and S5E). In *Nid1*$^{-/-}$ mice, both pSTAT5 and pro-B cell proliferation were decreased to the levels observed in WT pre-BI cells, and this was not due to reduced IL-7R expression levels (Figure S5F).

To exclude any contribution of Nidogen1 expressed by hematopoietic cells to the phenotype, wild-type BM was transplanted into lethally irradiated *Nid1*$^{-/-}$ mice (stroma knockout

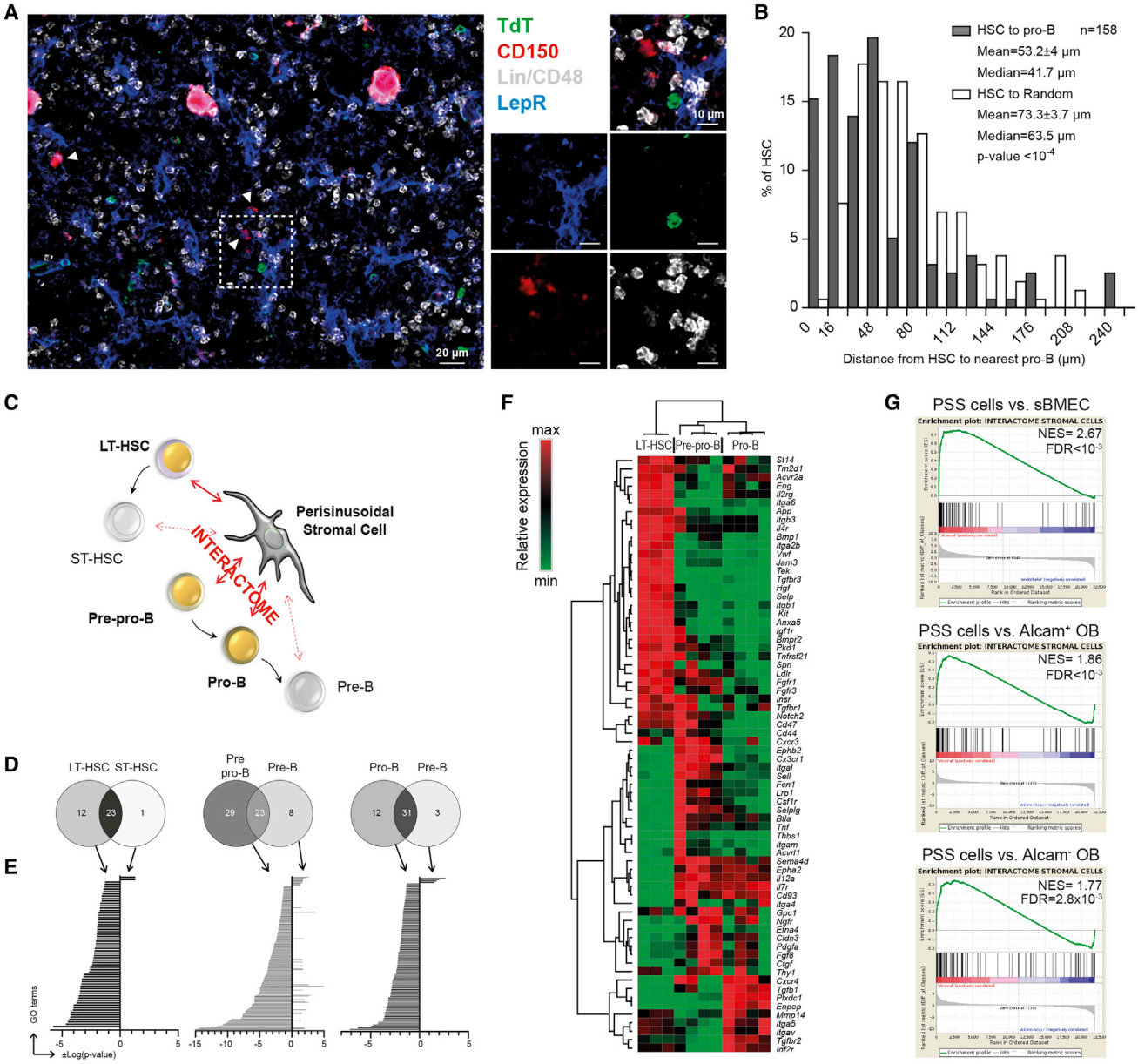

Figure 4. HSCs and Pro-B Cells Are Frequently Found in the Same Niche and Form Specific Interaction Networks with PSS Cells

(A) Immunostaining of pro-B cells (TdT$^+$) and HSCs (Lin$^-$CD48$^-$CD150$^+$; arrowhead) on bone sections of WT mice. The images were obtained from maximum-intensity projection of tile Z scans. The region in the dotted square was magnified for better visualization of the contact between a LepR$^+$ PSS cell, a HSC, and a pro-B cell (right). See also Video S1.

(B) Quantification in 3D of the distance between each HSC and the nearest pro-B or the nearest randomly positioned cell (n = 158) as indicated.

(C) Gene datasets for YFP$^+$ PSS cells from IL-7 reporter mice were compared to those of LT-HSCs, ST-HSCs, pre-pro-B cells, pro-B cells, and pre-B cells to generate the respective interactomes.

(D) Genes of the interactome expressed by LT-HSCs and by pre-pro-B or pro-B cells were compared to ST-HSCs and pre-B cells, respectively. The Venn diagrams display the number of upregulated genes for each of the indicated hematopoietic subsets.

(E) The genes overexpressed by each subset compared to their nearest related subset as defined in (D) were used to perform a functional profiling by defining the enrichment for particular GO annotations (arrows point to the corresponding histogram). GO terms are represented on the y axis and the significance on the x axis (±Log(p value); see also Table S3).

(F) Heatmap showing genes expressed by LT-HSCs, pre-pro-B cells, or pro-B cells and involved in the interactome with YFP$^+$ PSS cells. The fold-change for expression between extremes ranged from 1.7 to 31.8. Unsupervised clustering was performed on rows and columns.

(G) GSEA assessing enrichment of the stromal cell interactome as determined with LT-HSC, pre-pro-B, and pro-B, on the pairwise comparisons of PSS cells (red) with OBs (Alcam$^-$ or Alcam$^+$) or sBMECs (blue). NES, normalized enrichment score; FDR, false discovery rate. See also Figure S4.

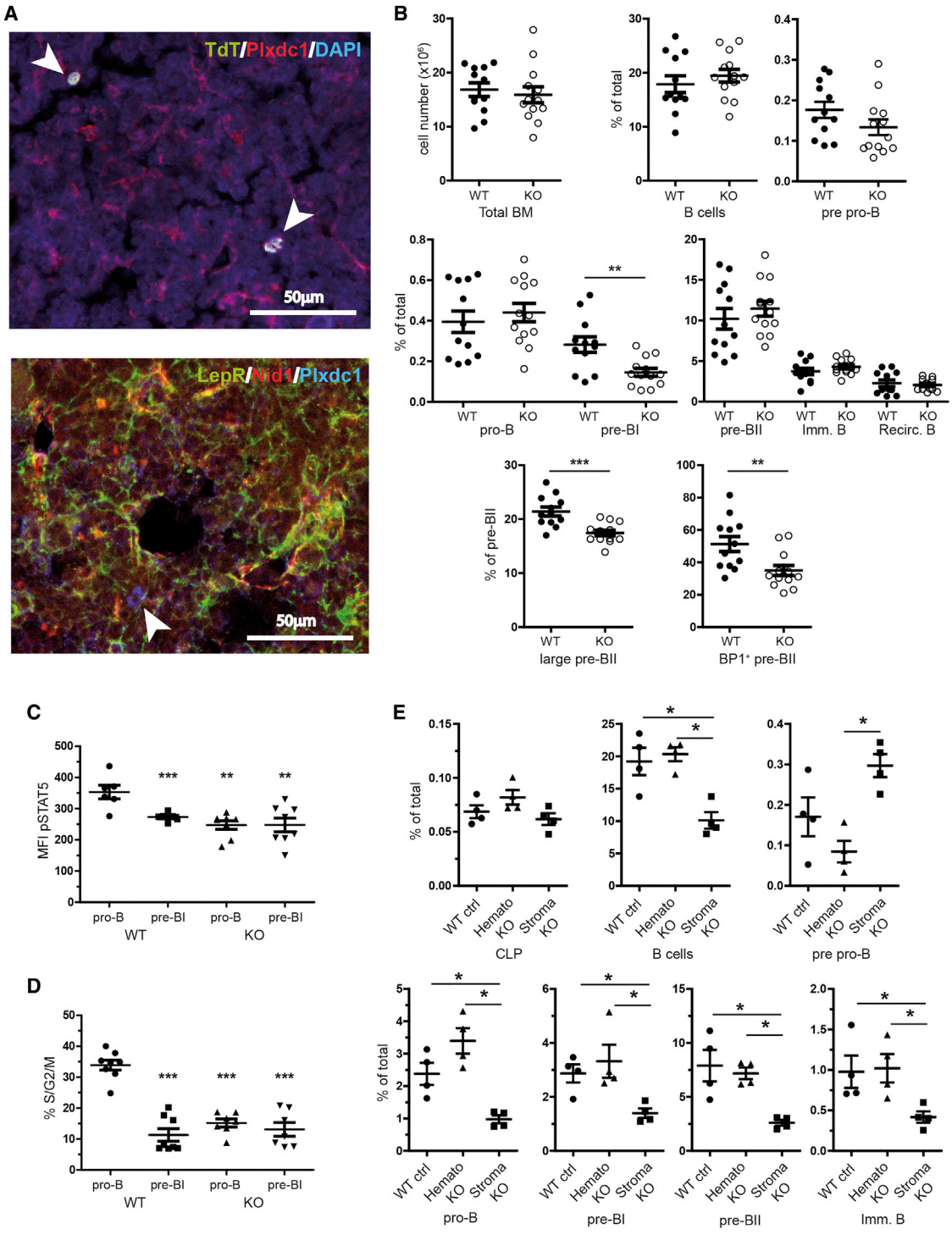

Figure 5. Nidogen-1 Allows Pro-B Cell Access to IL-7

(A) Maximum intensity projections of confocal images showing immunostaining for PLXDC1, TdT, and DAPI (top), or LepR, Nidogen-1, and PLXDC1 (top) on femoral sections. PLXDC1^{+} cells are shown with arrowheads.

(B) WT (n = 12) and Nid1$^{-/-}$ mice (n = 13) were analyzed by flow cytometry. The total cell number in the BM and the frequency of each B cell subset are shown.

(C) Mean fluorescence intensity (MFI) for pSTAT5 in the pro-B and pre-BI subsets from WT (n = 7) and Nid1$^{-/-}$ (n = 8) mice as assessed by flow cytometry.

(legend continued on next page)

[KO]) and B cell differentiation was compared to controls. While common lymphoid progenitor (CLP) frequency was similar between conditions, an accumulation of pre-pro-B cells was observed in stroma KO chimeras as compared to controls (Figure 5E). B cell differentiation was significantly decreased from the pro-B cell stage in the stroma KO chimeras only, confirming the importance of Nidogen-1 produced by the microenvironment for pro-B cell development.

Further analysis of Nidogen-1 immunostaining revealed that, in addition to sinusoidal expression (Figure 5A, bottom), bright signals were associated to arterioles (Figure 6A), consistent with *Nid1* expression in PSS cells and BMECs (Figure S6A). However, TdT$^+$ pro-B cells were found in close vicinity to Nid1$^+$LepR$^+$ PSS cells and mainly away from Nid1^{hi} arterioles (Figure 6A, bottom right). This localization was specific since randomly positioned cells were at a significantly greater distance from Nid1$^+$LepR$^+$ PSS cells but not from arterioles, suggesting that Nidogen-1 associated to PSS cells is necessary for pro-B cell localization in the peri-sinusoidal niche. This was confirmed by the finding that the distance between pro-B cells and LepR$^+$ PSS cells was significantly greater in *Nid1*$^{-/-}$ mice as compared to control (Figure 6B, bottom right).

In addition to pro-B cell localization with respect to LepR$^+$ cells, *Nid1* deficiency affected the structure of sinusoids (Figure 6B, insets). This was consistent with a change in H-type (Emcn^{hi}CD31^{hi}) vessel columns, which were much shorter and lacked a straight columnar organization in *Nid1*$^{-/-}$ mice (Figure S6B), as previously reported in vascular specific *itgb1*- and *Lama5*-deficient mice (Langen et al., 2017). However, this modification in vascular organization had no effect on early hematopoiesis from LT-HSCs to myeloid and lymphoid progenitors (Figure S5G). Of note, the LepR staining appeared more diffuse in *Nid1*$^{-/-}$ mice. This may be attributed to a decreased capacity of PSS cells to spread on the Nidogen-1-depleted extracellular matrix (ECM) surrounding sinusoids instead of PSS cell defects. Indeed, the relative proportions of LepR$^+$ PSS cells and pericytes were similar between *Nid1*$^{-/-}$ and WT mice, and PSS cells expressed normal LepR mRNA and protein levels (Figures S6C and S6D). In addition, *Nid1* deficiency did not affect expression of HSC or B cell niche genes (*Kitl*, *Cxcl12*, *Alpl*, *Angpt1*, *Il7*, *Vcam1*), *of Foxc1*, master regulator of the HSC niche (Omatsu et al., 2014), or of ECM genes (*Col1a1* and *Lama4*; Figure S6D). Finally, CXCR4 and CD49d (α4-integrin, VCAM1 ligand), shown to be crucial for B cell localization in the niche (Fistonich et al., 2018), were also normally expressed by pro-B cells in *Nid1*$^{-/-}$ mice. Altogether, these results suggest that Nidogen-1 regulates pro-B cell accessibility to IL-7-secreting PSS cells.

Human Pro-B Cells and HSPC Localize Close to a Human Stromal Cell Subset Related to the Murine PSS Cell Niche

Similarly to murine PSS cells, stromal cells expressing CD54, LepR, and CD317, which represent 1%–3% of low-passage BM mesenchymal cells, have recently been identified in human BM samples (James et al., 2015). In addition, and in opposition to CD317$^-$ mesenchymal cells, human primary CD317$^+$ cells express high levels of IL-7 at the transcript and protein level. We thus compared gene expression profiles of murine PSS cells to the published datasets from CD317$^+$IL-7^{hi} (Y102 and Y202 cell lines) and CD317$^-$IL-7^{lo} (Y101 and Y201 cell lines) human stromal cells (James et al., 2015). Unsupervised PCA analysis showed that mouse PSS cells clustered together with human IL-7^{hi} stromal cells (Figure 7A, top). Furthermore, when PCA was restricted to the genes identified in murine PSS cells by the interactome approach, the distinction between IL-7^{lo} and IL-7^{hi} cells was even greater (Figure 7A, bottom).

This similarity between mouse and human CD317$^+$IL-7^{hi} cells prompted us to analyze their distribution in human primary BM samples and their localization relative to pro-B cells and HSPC. We therefore analyzed expression of CD317, IL-7, and CXCL12, and compared these patterns to CD34 expression, which stains HSPCs and endothelial cells. Cells expressing CD317, IL-7, and CXCL12 were localized close to CD34$^+$ endothelial cells (Figures 7B and S7). As expected, strong interstitial staining was observed for CXCL12. Most remarkably, in some cases we observed highly vascularized regions with strong expression of CD317, IL-7, and CXCL12 (Figure 7B, bottom). In agreement with results obtained in mouse tissue, TdT$^+$ pro-B cells were localized close to vessels and IL-7-expressing cells, and their frequency correlated with levels of IL-7 expression. Interestingly, like mouse pro-B cells, human pro-B cells also expressed PLXDC1 (Figure 7C). Finally, CD34$^+$ HSPCs were also observed in contact with IL-7$^+$ cells, sometimes in close proximity to pro-B cells (Figures 7B and S7B). Overall, our results demonstrate that PSS cells secreting IL-7 and CXCL12 exist in humans and present a very similar gene expression profile to the mouse PSS subpopulation, suggesting that a number of biological questions related to leuko/stromal cross talk could be addressed across multiple species.

DISCUSSION

In the present study, we have developed antibody panels for flow cytometry to visualize and isolate different stromal cell subpopulations from WT mice. Such a phenotypic characterization is useful to precisely quantify the specificity of the different Cre recombinase reporter systems that have been used to analyze BM niches in the past. Our analysis indicates that BM mesenchymal cells are limited to four subsets: MSCs, pericytes, PSS cells, and OBs. Although the existence of minor subsets cannot be excluded, this result considerably reduces the number of mesenchymal subsets described using various Cre recombinase reporter systems and thus of potential hematopoietic niches. We have found that PSS cells are the main IL-7-expressing cells (Mourcin et al., 2011), even though a small fraction of

(D) Proportion of pro-B and pre-BI cells from WT (n = 8) and Nid1$^{-/-}$ (n = 7) mice engaged in the S/G2/M phases of the cell cycle. Cell cycle analysis was performed by flow cytometry using TO-PRO3.

(E) B cell development analysis in the BM of stroma KO chimeras (WT donor BM transplanted to Nid1$^{-/-}$ mice) compared to WT control (WT into WT) and hemato KO chimeras (Nid1$^{-/-}$ into WT). n = 4 mice for each condition. Error bars represent SEM. Statistical significance was calculated using an unpaired t test. *p < 0.05; **p < 0.01; ***p < 0.001. See also Figure S5.

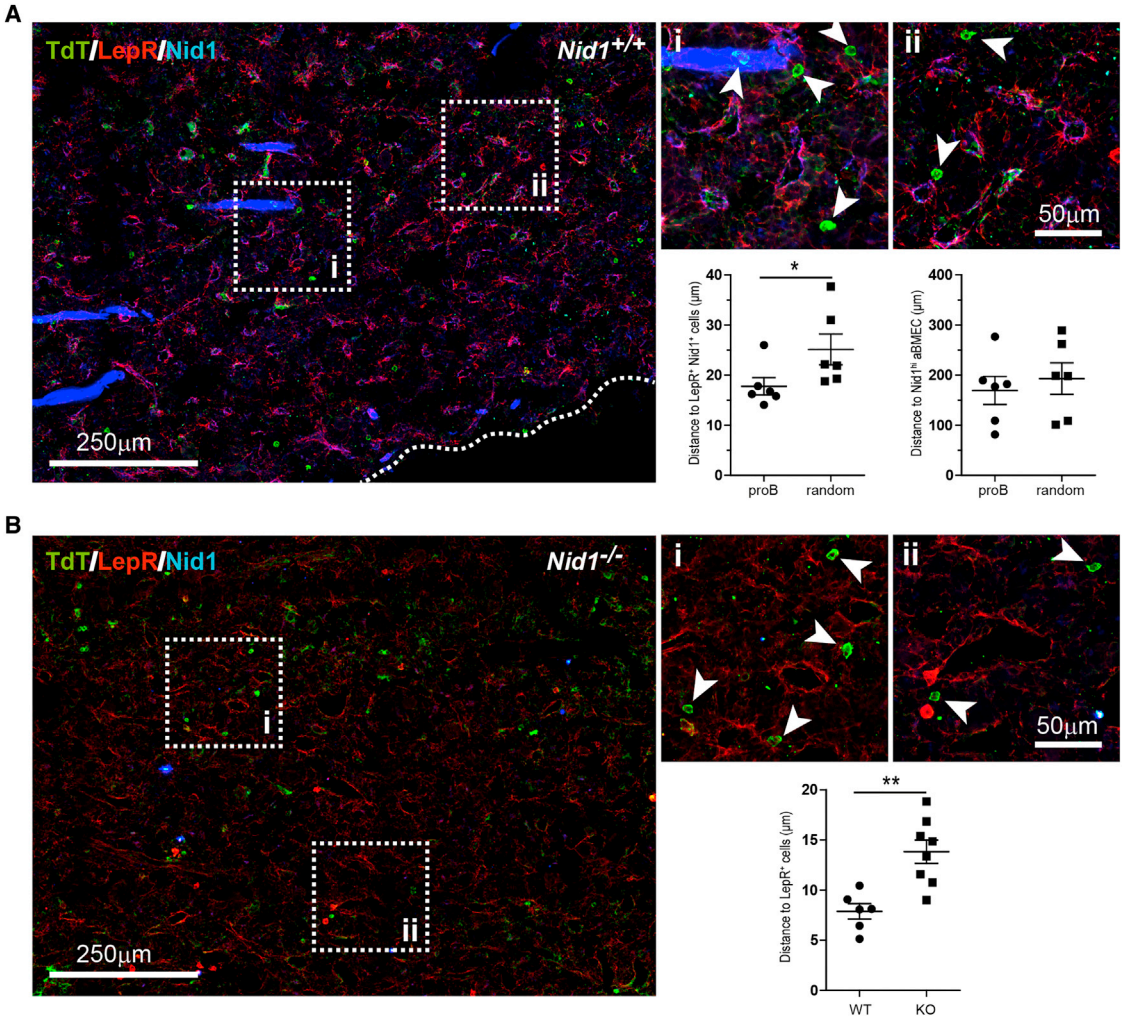

Figure 6. Nidogen-1 Allows Pro-B Cell Retention in the PSS Niche

(A and B) Maximum-intensity projections of tile scan confocal images showing Nidogen-1 (blue), TdT$^+$ (green), and LepR$^+$ (red) immunostaining of bone sections from WT (A) and Nid1$^{-/-}$ mice (B). Pro-B cells are indicated with arrowheads, and dashed lines delineate the bone border.

(A) Lower right charts show 3D quantitation of the distance between TdT$^+$ pro-B cells and LepR$^+$Nid1$^+$ PSS cells as well as between TdT$^+$ pro-B cells and Nid1^{hi} arterioles. Results are expressed as the average distance per mouse (n = 6) and compared to the distance measured after random positioning of pro-B cells.

(B) The lower right chart shows 3D quantitation of the distance between pro-B cells and LepR$^+$ cells in WT and *Nid1*$^{-/-}$ mice. Results are expressed as the average distance per mouse (*Nid1*$^{+/+}$, n = 6; *Nid1*$^{-/-}$. n = 8). Error bars represent SEM. Statistical significance was calculated using an unpaired t test. *p = 0.026; **p = 0.0019.

OBs and pericytes expressed IL-7-Cre/YFP reporter but not *Il7*. Because OBs differentiate from PSS cells in adult life only (Mizoguchi et al., 2014) and do not express YFP in 2- to 3-week-old IL-7 reporter mice, we can assume that YFP expression in adult OBs is due to IL-7-driven Cre recombinase expression in PSS osteo-progenitors. Similar results were reported by Pereira and colleagues (Cordeiro Gomes et al., 2016). In the case of pericytes, the partial recombination that we observed at the Rosa-YFP locus may be due to *Il7* expression at levels below the qPCR detection threshold. Indeed, RNA-seq studies previously indicated very low levels of *IL-7* in pericytes (Kunisaki et al., 2013). Similarly, we did not detect IL-7-Cre reporter expression in endothelial cells (Figures 2 and S3), although one study reported detectable *Il7* transcript expression in BMECs (Cordeiro Gomes et al., 2016). We believe that this is due to very low activity of Il7 promoter in endothelial cells, since BMECs were shown to express 20-fold less IL-7 than PSS cells. Approximately 60% of PSS cells were found to be YFP$^+$ using the IL-7 reporter system (Figure 2C), suggesting that IL-7-expressing cells represent a subset of PSS cells. However, YFP$^+$ and YFP$^-$ fractions were identical at the transcriptomic level, and both expressed *Il7* (Figures 3A and 3B). This effect is most likely due to low Cre recombinase expression under the control of the IL-7 promoter, as already reported by others (Alves et al., 2009; Mazzucchelli et al., 2009). Indeed, conditional deletion of Cxcl12 using the Il7-Cre or the LepR-Cre systems led to a decrease in HSCs in

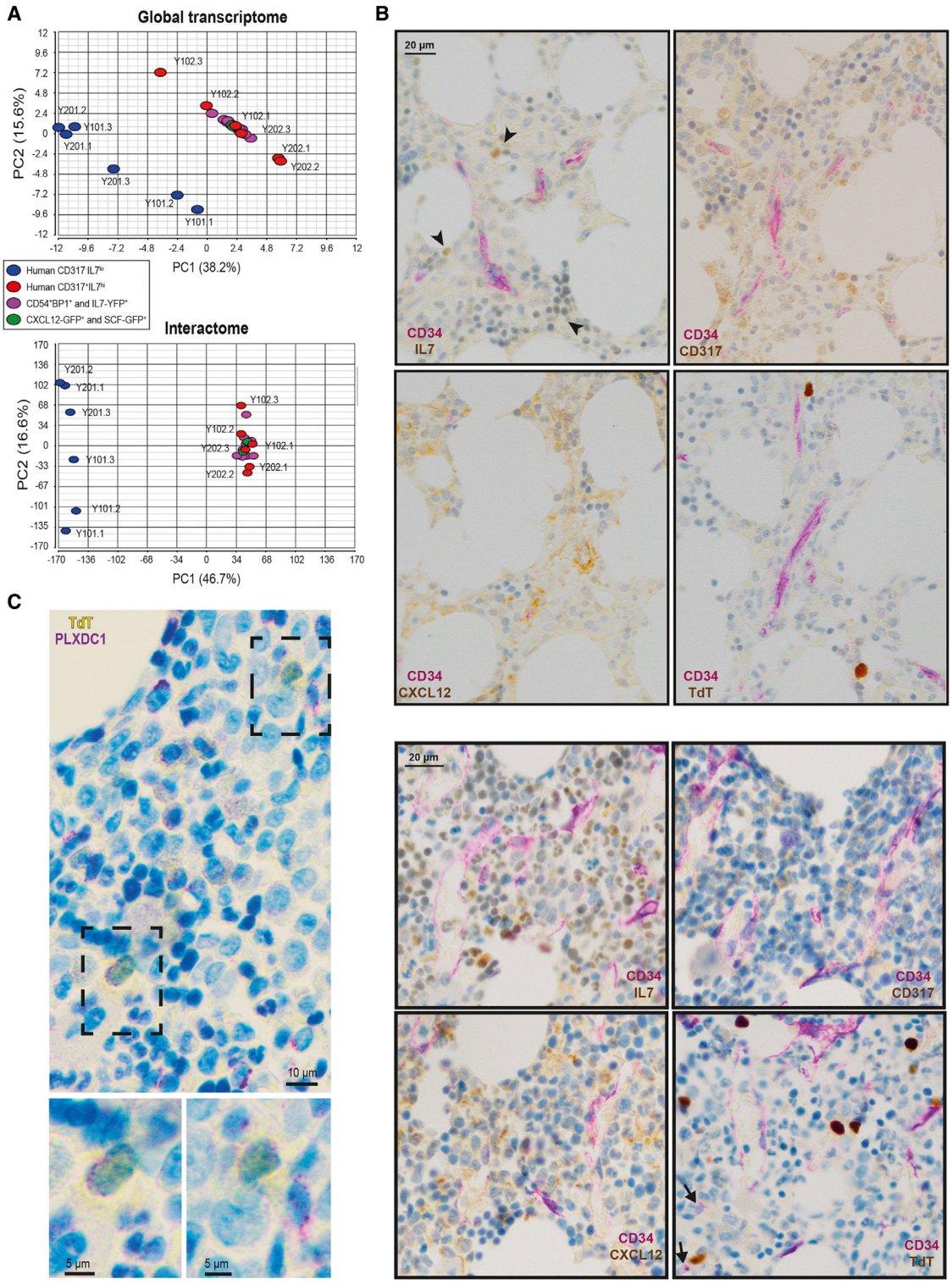

Figure 7. Human IL-7-Expressing Cells Are Very Similar to Mouse PSS Cells and Are in Contact with Pro-B Cells and HSPCs

(A) PCA of murine PSS cells with human CD317^{+}IL-7^{hi} and CD317^{-}IL-7^{lo} stromal cells with all expressed genes in mouse and human (top) or with genes identified from PSS cell interactome with LT-HSC, pre-pro-B, and pro-B (top).

(B) Immunohistochemistry (IHC) was performed on human BM sections using anti-CD34, anti-CD317, anti-IL-7, anti-CXCL12, and anti-TdT antibodies (see controls in Figure S7A). Immunostainings were performed on serial sections. Top and bottom panels correspond to sections from two different samples.

(legend continued on next page)

the BM with both Cre systems, but loss of retention was only observed in the LepR-Cre system. This difference has been attributed to a differential role of CXCL12 produced by IL-7$^+$ compared to IL-7$^-$ PSS cells (Cordeiro Gomes et al., 2016). Based on our observations, it rather appears that CXCL12 deletion is more efficient in LepR-Cre than in IL-7-Cre mice and thus that a slight variation in CXCL12 levels has a more dramatic effect on HSC maintenance than on their retention in the BM.

Having established the nature of IL-7-expressing cells, we examined the localization of pro-B cells, which strongly rely on IL-7 for their development. Pro-B cells were mainly distributed in the conduit close to LepR$^+$ PSS cells, and away from the endosteum, suggesting that OBs do not play a prominent role in B cell differentiation as previously thought (Wu et al., 2008; Zhu et al., 2007). This apparent discrepancy is most probably due to the fact that the systems used to specifically induce gene deletion in OBs such as Osx-Cre or Bglap-Cre mice were also inducing deletion in PSS osteo-progenitors (Mizoguchi et al., 2014; Zhang and Link, 2016). Alternatively, some systems may affect PSS cells indirectly. Acute ablation of OBs using thymidine kinase under the control of the Col1a1 promoter (Col2.3ΔTK) leads to decreased numbers of early B cells (Zhu et al., 2007). In this system, it is possible that a massive loss of OBs triggers PSS cell differentiation, which affects the hematopoietic compartment as described in another study (Visnjic et al., 2004). Finally, one could not exclude that PSS cells are directly ablated in this system since they express Col1a1 (Figure 3C).

Through our interactome analysis, we identified Nidogen-1, expressed by PSS cells, as a regulator of pro-B cell positioning with respect to the LepR-expressing peri-sinusoidal niche. Although the vascular structure is modified in *Nid1*$^{-/-}$ mice and the abundance of LepR$^+$ structures seems affected, an indirect effect on pro-B cell differentiation is unlikely. Indeed, HSCs, which strongly rely on secretion of CXCL12 and SCF by BMECs for their maintenance (Asada et al., 2017; Xu et al., 2018), are not affected, and the frequency of PSS cells as well as their expression of crucial HSC and B cell niche genes were not altered in *Nid1*$^{-/-}$ mice. More specifically, PSS and pro-B cells from deficient animals express, respectively, normal levels of CXCL12/VCAM1 and of their respective ligands CXCR4/α4-integrin, shown to be crucial for pro-B retention in the niche (Arroyo et al., 1996; Park et al., 2013). In addition, adoptive transfer experiments show that the pro-B cell defect is not cell-autonomous, suggesting that CXCR4 and α4-integrin signaling may be necessary but not sufficient to explain pro-B cell retention in the niche. On the other hand, we cannot exclude a contribution of endothelial cells in the formation of the matrix surrounding the PSS cells since Nidogen-1 is expressed by BMECs. However, pro-B cells do not preferentially localize close to Nid1^{hi} arterioles, indicating that Nidogen-1 expression is not sufficient to sustain B cell development. Instead, we believe that a complex network of factors and signaling, involving Nidogen-1, CXCL12, and VCAM1, is required for localization of pro-B cells near IL-7-producing PSS cells.

It is known that cultured pro-B cells need high concentrations of IL-7 to proliferate, while decreasing IL-7 concentration induces differentiation toward the pre-BI stage, V-to-DJ recombination, and intracellular expression of IgH chains (Marshall et al., 1998). Early B cells lose their dependency on IL-7 at the pre-BCR$^+$ pre-BII stage, as they mature toward the immature B cell stage. In line with these observations, we found that WT pro-B cells proliferate more than pre-BI cells (Figure 5). When pro-B cells are far from the PSS niche, as is the case in *Nid1*$^{-/-}$ mice, their proliferation rate is decreased to the level of pre-BI cells. This suggests that pro-B cells need to move away from the source of IL-7 to differentiate into pre-BI cells, as also supported by recent studies in which the amount of IL-7 in the peri-sinusoidal niche or the integrin-mediated adhesion of pro-B cells were manipulated (Cordeiro Gomes et al., 2016; Fistonich et al., 2018).

Our results and others suggest that distance of hematopoietic cells to their niche is important for their development (Cordeiro Gomes et al., 2016; Itkin et al., 2016; Kunisaki et al., 2013; Mourcin et al., 2011; Tokoyoda et al., 2004). However, as LepR$^+$ stromal cells are widespread in the BM, we cannot exclude the presence of fine reticular extensions of PSS cells deeper in the parenchyma. These extensions may be implicated in the chemokine or growth factor gradients that are formed along cell surface in association with the ECM (Laguri et al., 2008). On the other hand, our interactome analysis confirms that accessibility of hematopoietic cells to a specific niche is related not only to distance per se but also to the capacity to form specific interaction networks. As an example, pro-B cells expressed a higher number of genes involved in the interaction with PSS than pre-B cells, which are known to be associated with distinct Gal1$^+$ stromal cells (Figure 4D). This would be consistent with recent results showing that a fraction of motile pre-B cells are located close to peri-sinusoidal niches but do not engage stable interactions with PSS cells (Fistonich et al., 2018). We can then speculate that both the distance to the sinusoidal regions and adhesion to stromal cells or ECM are important for hematopoietic differentiation.

Our work not only shows the influence of PSS cells on early B cell development but also asks the question of BM compartmentalization and niche specificity. A PCA performed previously showed the proximity of the different known PSS cell subsets using Nes-GFP and SCF-GFP reporter mice and their distance from other mesenchymal subsets (Isern et al., 2014). We now confirm at the single-cell level that PSS cells form a homogeneous cluster distinct from BMECs, pericytes, OBs, or MSCs. However, because of technological limitations due to the detection of the most abundant poly(A) RNA only, we cannot rule out that a certain degree of intrinsic heterogeneity exists in the PSS cluster. For example, since it is known that PSS cells can differentiate in OBs and adipocytes, we cannot exclude that

IL-7$^+$ cells are shown with arrowheads. Hematopoietic stem and progenitor cells (HSPCs) are indicated by an arrow in the CD34/TdT co-staining to show their proximity to both CD34$^+$ vessels and TdT$^+$ pro-B cells. Large fields from which the bottom panels were extracted are presented in Figure S7B.
(C) IHC was performed on human bone sections using anti-TdT and anti-PLXDC1 antibodies. Hematoxylin was used as counterstain. The regions in the dotted squares were magnified to better visualize PLXDC1/TdT co-staining (bottom).

PSS cells engaged in differentiation contribute to undetected intrinsic cluster heterogeneity. However, this should concern only a limited number of PSS cells and genes since the cluster is clearly homogeneous for the expression of a large number of genes (Table S1). Moreover, in addition to the maintenance of HSCs through secretion of both SCF and CXCL12 (Ding and Morrison, 2013; Ding et al., 2012; Greenbaum et al., 2013; Sugiyama et al., 2006) and of pre-pro-B cells through secretion of CXCL12 (Ding and Morrison, 2013; Greenbaum et al., 2013; Tokoyoda et al., 2004), our results demonstrate that the same PSS cells sustain pro-B cells. Most importantly, HSCs can be found together with pro-B cells in the same niche. Even if there is competition to access factors such as CXCL12 (by HSC, pre-pro-B, and pro-B) or IL-7 (by pre-pro-B and pro-B), HSCs specifically interact with PSS cells through expression of "HSC niche genes," while early B cells engage specific interactions by upregulating "lymphoid niche genes." As a result, PSS cells appear to be able to accommodate different hematopoietic cells by supplying the appropriate crucial niche factors required for the development of distinct lineages.

In addition to HSCs, pre-pro-B cells, and pro-B cells, other hematopoietic subsets are also associated with sinusoids. Indeed, plasma cells have been shown to be in contact with peri-sinusoidal CAR cells and to rely on CXCL12, CD54, and CD106 for homing and maintenance in the BM (DiLillo et al., 2008; Tokoyoda et al., 2004). More recently, multi-potent progenitors (MPPs) and CLPs were also found associated with PSS cells (Cordeiro Gomes et al., 2016). Results from this study demonstrated that CXCL12 favors positioning of CLP close to PSS to gain access to IL-7, suggesting that PSS cells organize hematopoietic cell positioning in the BM. This capacity of PSS cells to accommodate hematopoietic cells at distinct stages of development fits with the hemosphere model proposed earlier (Wang et al., 2013). In their study, Adams and colleagues described HSCs forming units with both mesenchymal and endothelial cells. Interestingly, this specific niche allowed local clonal expansion of HSCs into more mature hematopoietic lineages. In line with this organization, we found that half of the HSCs were located at less than 41.7 μm from pro-B cells, suggesting that factors involved in the development of distinct hematopoietic subsets are supplied locally and that migration of developing cells relative to mother cell is relatively limited.

Although increasing evidence demonstrates the localization of numerous hematopoietic subsets close to sinusoids, this does not preclude the existence of other cellular niches. Indeed, arteriolar Nestin$^+$ stromal cells have been shown to maintain HSCs into quiescence (Kunisaki et al., 2013). In addition, the low permeability of arteries as compared to sinusoids would be a favorable niche for HSC quiescence through the maintenance of low reactive oxygen species levels (Itkin et al., 2016). Finally, CXCL12 and SCF expression by aBMECs is crucial for HSC maintenance (Xu et al., 2018). According to these results, it can be proposed that, in order to differentiate, quiescent HSCs enter the G1 phase of the cycle but retain their capacity to self-renew, while moving from the arteriolar to the sinusoidal niche. Once in the sinusoidal region, the HSCs will find growth factors allowing both their maintenance and their commitment into distinct lineages.

Although considerable knowledge has been acquired with respect to murine stromal cell niches *in situ* over recent years, less is known in humans. Comparison of the transcriptomic profiles for murine PSS cells with IL-7^{hi} stromal cells isolated from human BM revealed a close relationship between them. Furthermore, human IL-7^{hi} cells expressed genes involved in murine PSS cell interactions with HSCs and early B cells, indicating that they probably share the capacity to accommodate distinct hematopoietic subsets, as already suggested by the preferential localization of CD34$^+$ progenitors in the vicinity of PSS cells (Tormin et al., 2011). We confirmed CD317, IL-7, and CXCL12 expression by human PSS cells *in situ*, and identified TdT$^+$ pro-B cells and CD34$^+$ HSPCs in close vicinity. In addition, we observed that pro-B cells were more frequently associated with IL-7-rich regions, suggesting that human pro-B cells are also dependent on IL-7. This finding appears to contradict older studies that suggested that IL-7 was not required for human B cell development since B cells were present in SCID patients where no IL-7R signaling occurs (Russell et al., 1995). However, more recently, it was shown that IL-7 induces human pro-B cell proliferation, suggesting that the B cells found in SCID patients correspond to a wave of IL-7-independent fetal B cells (Bendall et al., 2014; Johnson et al., 2005; Milford et al., 2016).

In conclusion, our results demonstrate that murine and human PSS cells specifically supply niche factors required for HSC and early B cell developmental programs. Although mesenchymal cells are certainly heterogeneous, our results demonstrate that hematopoietic niches in the BM can be multifunctional and that their number may be lower than previously thought. Finally, the existence of a similar niche in humans will have considerable impact on the development of regenerative medicine aiming to manipulate hematopoietic differentiation in pathological situations.

STAR★METHODS

Detailed methods are provided in the online version of this paper and include the following:

- KEY RESOURCES TABLE
- CONTACT FOR REAGENT AND RESOURCE SHARING
- EXPERIMENTAL MODEL AND SUBJECT DETAILS
  - Mice
  - Human tissues
- METHOD DETAILS
  - Flow cytometry and cell sorting
  - Immunohistofluorescence
  - Quantification of confocal images
  - Immunohistochemistry
  - Gene expression profiling
  - Microarray analysis
  - Interactome analysis
- QUANTIFICATION AND STATISTICAL ANALYSIS
- DATA AND SOFTWARE AVAILABILITY

SUPPLEMENTAL INFORMATION

Supplemental Information can be found with this article online at https://doi.org/10.1016/j.celrep.2019.02.065.

ACKNOWLEDGMENTS

We are grateful to the core flow cytometry and the animal and microscopy facilities of the CRCM and CIML for providing supportive help, to Prof. Thomas Krieg for the kind gift of important material, and to Emilie Agavnian from the ICEP platform for technical help. This work was partly supported by grants from the SIRIC (Inca-Inserm-DGOS 6038), the Cancéropôle PACA funded by Inca, the ARC Foundation (PJA#20131200298 and PJA#20161204555 to S.J.C.M.; PJA#20141201990 to M.A.-L.), the ANR (OSTEOVALYMPH, ANR-17-CE14-0019-03), and the Excellence Initiative of Aix-Marseille University–A*MIDEX, a French "Investissements d'Avenir" program. M. Balzano was the recipient of a PhD grant from FRM (#FDT20150532380); M.D.G.'s postdoctoral fellowship was supported by the Fondation de France (#2013-00042638).

AUTHOR CONTRIBUTIONS

Conceptualization, M.A.-L., C.S., and S.J.C.M.; Methodology, M. Balzano, M.D.G., M.A.-L., and S.J.C.M.; Validation, M. Balzano, M.D.G., M.A.-L., and S.J.C.M.; Formal Analysis, T.-P.V.M., A.S., G.B., P.C., L.H., and S.J.C.M.; Investigation, M. Balzano, M.D.G., T.-P.V.M., L.C., F.B., A.F., A.S., A.-L.B., A.C.-M., A.B., L.H., M.A.-L., and S.J.C.M.; Resources, M.D., E.D., P.G., M.C., M. Bajenoff, and L.X.; Data Curation, T.-P.V.M., A.S., G.B., P.C., and L.H.; Writing – Original Draft, S.J.C.M.; Writing – Review & Editing, M.A.-L., C.S., and S.J.C.M.; Supervision, M.A.-L., C.S., and S.J.C.M.; Funding Acquisition, M.A.-L. and S.J.C.M.

DECLARATION OF INTERESTS

The authors declare no competing interests.

Received: April 20, 2018
Revised: December 24, 2018
Accepted: February 15, 2019
Published: March 19, 2019

REFERENCES

Alves, N.L., Richard-Le Goff, O., Huntington, N.D., Sousa, A.P., Ribeiro, V.S., Bordack, A., Vives, F.L., Peduto, L., Chidgey, A., Cumano, A., et al. (2009). Characterization of the thymic IL-7 niche in vivo. Proc. Natl. Acad. Sci. USA *106*, 1512–1517.

Arroyo, A.G., Yang, J.T., Rayburn, H., and Hynes, R.O. (1996). Differential requirements for alpha4 integrins during fetal and adult hematopoiesis. Cell *85*, 997–1008.

Asada, N., Kunisaki, Y., Pierce, H., Wang, Z., Fernandez, N.F., Birbrair, A., Ma'ayan, A., and Frenette, P.S. (2017). Differential cytokine contributions of perivascular haematopoietic stem cell niches. Nat. Cell Biol. *19*, 214–223.

Aurrand-Lions, M., and Mancini, S.J.C. (2018). Murine bone marrow niches from hematopoietic stem cells to B cells. Int. J. Mol. Sci. *19*, 2353.

Bendall, S.C., Davis, K.L., Amir, A.D., Tadmor, M.D., Simonds, E.F., Chen, T.J., Shenfeld, D.K., Nolan, G.P., and Pe'er, D. (2014). Single-cell trajectory detection uncovers progression and regulatory coordination in human B cell development. Cell *157*, 714–725.

Charbord, P., Pouget, C., Binder, H., Dumont, F., Stik, G., Levy, P., Allain, F., Marchal, C., Richter, J., Uzan, B., et al. (2014). A systems biology approach for defining the molecular framework of the hematopoietic stem cell niche. Cell Stem Cell *15*, 376–391.

Cordeiro Gomes, A., Hara, T., Lim, V.Y., Herndler-Brandstetter, D., Nevius, E., Sugiyama, T., Tani-Ichi, S., Schlenner, S., Richie, E., Rodewald, H.R., et al. (2016). Hematopoietic stem cell niches produce lineage-instructive signals to control multipotent progenitor differentiation. Immunity *45*, 1219–1231.

Dai, M., Wang, P., Boyd, A.D., Kostov, G., Athey, B., Jones, E.G., Bunney, W.E., Myers, R.M., Speed, T.P., Akil, H., et al. (2005). Evolving gene/transcript definitions significantly alter the interpretation of GeneChip data. Nucleic Acids Res. *33*, e175.

Decker, M., Martinez-Morentin, L., Wang, G., Lee, Y., Liu, Q., Leslie, J., and Ding, L. (2017). Leptin-receptor-expressing bone marrow stromal cells are myofibroblasts in primary myelofibrosis. Nat. Cell Biol. *19*, 677–688.

Dias, S., Silva, H., Jr., Cumano, A., and Vieira, P. (2005). Interleukin-7 is necessary to maintain the B cell potential in common lymphoid progenitors. J. Exp. Med. *201*, 971–979.

DiLillo, D.J., Hamaguchi, Y., Ueda, Y., Yang, K., Uchida, J., Haas, K.M., Kelsoe, G., and Tedder, T.F. (2008). Maintenance of long-lived plasma cells and serological memory despite mature and memory B cell depletion during CD20 immunotherapy in mice. J. Immunol. *180*, 361–371.

Ding, L., and Morrison, S.J. (2013). Haematopoietic stem cells and early lymphoid progenitors occupy distinct bone marrow niches. Nature *495*, 231–235.

Ding, L., Saunders, T.L., Enikolopov, G., and Morrison, S.J. (2012). Endothelial and perivascular cells maintain haematopoietic stem cells. Nature *481*, 457–462.

Egawa, T., Kawabata, K., Kawamoto, H., Amada, K., Okamoto, R., Fujii, N., Kishimoto, T., Katsura, Y., and Nagasawa, T. (2001). The earliest stages of B cell development require a chemokine stromal cell-derived factor/pre-B cell growth-stimulating factor. Immunity *15*, 323–334.

Espeli, M., Mancini, S.J., Breton, C., Poirier, F., and Schiff, C. (2009). Impaired B-cell development at the pre-BII-cell stage in galectin-1-deficient mice due to inefficient pre-BII/stromal cell interactions. Blood *113*, 5878–5886.

Fistonich, C., Zehentmeier, S., Bednarski, J.J., Miao, R., Schjerven, H., Sleckman, B.P., and Pereira, J.P. (2018). Cell circuits between B cell progenitors and IL-7^{+} mesenchymal progenitor cells control B cell development. J. Exp. Med. *215*, 2586–2599.

Garcia, M., Finetti, P., Bertucci, F., Birnbaum, D., and Bidaut, G. (2014). Detection of driver protein complexes in breast cancer metastasis by large-scale transcriptome-interactome integration. Methods Mol. Biol. *1101*, 67–85.

Greenbaum, A., Hsu, Y.M., Day, R.B., Schuettpelz, L.G., Christopher, M.J., Borgerding, J.N., Nagasawa, T., and Link, D.C. (2013). CXCL12 in early mesenchymal progenitors is required for haematopoietic stem-cell maintenance. Nature *495*, 227–230.

Heng, T.S., and Painter, M.W.; Immunological Genome Project Consortium (2008). The Immunological Genome Project: networks of gene expression in immune cells. Nat. Immunol. *9*, 1091–1094.

Isern, J., García-García, A., Martín, A.M., Arranz, L., Martín-Pérez, D., Torroja, C., Sánchez-Cabo, F., and Méndez-Ferrer, S. (2014). The neural crest is a source of mesenchymal stem cells with specialized hematopoietic stem cell niche function. eLife *3*, e03696.

Itkin, T., Gur-Cohen, S., Spencer, J.A., Schajnovitz, A., Ramasamy, S.K., Kusumbe, A.P., Ledergor, G., Jung, Y., Milo, I., Poulos, M.G., et al. (2016). Distinct bone marrow blood vessels differentially regulate haematopoiesis. Nature *532*, 323–328.

James, S., Fox, J., Afsari, F., Lee, J., Clough, S., Knight, C., Ashmore, J., Ashton, P., Preham, O., Hoogduijn, M., et al. (2015). Multiparameter analysis of human bone marrow stromal cells identifies distinct immunomodulatory and differentiation-competent subtypes. Stem Cell Reports *4*, 1004–1015.

Johnson, S.E., Shah, N., Panoskaltsis-Mortari, A., and LeBien, T.W. (2005). Murine and human IL-7 activate STAT5 and induce proliferation of normal human pro-B cells. J. Immunol. *175*, 7325–7331.

Kiel, M.J., Yilmaz, O.H., Iwashita, T., Yilmaz, O.H., Terhorst, C., and Morrison, S.J. (2005). SLAM family receptors distinguish hematopoietic stem and progenitor cells and reveal endothelial niches for stem cells. Cell *121*, 1109–1121.

Kunisaki, Y., Bruns, I., Scheiermann, C., Ahmed, J., Pinho, S., Zhang, D., Mizoguchi, T., Wei, Q., Lucas, D., Ito, K., et al. (2013). Arteriolar niches maintain haematopoietic stem cell quiescence. Nature *502*, 637–643.

Kusumbe, A.P., Ramasamy, S.K., and Adams, R.H. (2014). Coupling of angiogenesis and osteogenesis by a specific vessel subtype in bone. Nature *507*, 323–328.

Kusumbe, A.P., Ramasamy, S.K., Starsichova, A., and Adams, R.H. (2015). Sample preparation for high-resolution 3D confocal imaging of mouse skeletal tissue. Nat. Protoc. *10*, 1904–1914.

Laguri, C., Arenzana-Seisdedos, F., and Lortat-Jacob, H. (2008). Relationships between glycosaminoglycan and receptor binding sites in chemokines-the CXCL12 example. Carbohydr. Res. *343*, 2018–2023.

Langen, U.H., Pitulescu, M.E., Kim, J.M., Enriquez-Gasca, R., Sivaraj, K.K., Kusumbe, A.P., Singh, A., Di Russo, J., Bixel, M.G., Zhou, B., et al. (2017). Cell-matrix signals specify bone endothelial cells during developmental osteogenesis. Nat. Cell Biol. *19*, 189–201.

Lee, H.K., Seo, I.A., Park, H.K., and Park, H.T. (2006). Identification of the basement membrane protein nidogen as a candidate ligand for tumor endothelial marker 7 in vitro and in vivo. FEBS Lett. *580*, 2253–2257.

Lee, N.J., Ali, N., Zhang, L., Qi, Y., Clarke, I., Enriquez, R.F., Brzozowska, M., Lee, I.C., Rogers, M.J., Laybutt, D.R., et al. (2018). Osteoglycin, a novel coordinator of bone and glucose homeostasis. Mol. Metab. *13*, 30–44.

Ma, Q., Jones, D., Borghesani, P.R., Segal, R.A., Nagasawa, T., Kishimoto, T., Bronson, R.T., and Springer, T.A. (1998). Impaired B-lymphopoiesis, myelopoiesis, and derailed cerebellar neuron migration in CXCR4- and SDF-1-deficient mice. Proc. Natl. Acad. Sci. USA *95*, 9448–9453.

Ma, Q., Jones, D., and Springer, T.A. (1999). The chemokine receptor CXCR4 is required for the retention of B lineage and granulocytic precursors within the bone marrow microenvironment. Immunity *10*, 463–471.

Macosko, E.Z., Basu, A., Satija, R., Nemesh, J., Shekhar, K., Goldman, M., Tirosh, I., Bialas, A.R., Kamitaki, N., Martersteck, E.M., et al. (2015). Highly parallel genome-wide expression profiling of individual cells using nanoliter droplets. Cell *161*, 1202–1214.

Marshall, A.J., Fleming, H.E., Wu, G.E., and Paige, C.J. (1998). Modulation of the IL-7 dose-response threshold during pro-B cell differentiation is dependent on pre-B cell receptor expression. J. Immunol. *161*, 6038–6045.

Mazzucchelli, R.I., Warming, S., Lawrence, S.M., Ishii, M., Abshari, M., Washington, A.V., Feigenbaum, L., Warner, A.C., Sims, D.J., Li, W.Q., et al. (2009). Visualization and identification of IL-7 producing cells in reporter mice. PLoS ONE *4*, e7637.

Méndez-Ferrer, S., Michurina, T.V., Ferraro, F., Mazloom, A.R., Macarthur, B.D., Lira, S.A., Scadden, D.T., Ma'ayan, A., Enikolopov, G.N., and Frenette, P.S. (2010). Mesenchymal and haematopoietic stem cells form a unique bone marrow niche. Nature *466*, 829–834.

Milford, T.A., Su, R.J., Francis, O.L., Baez, I., Martinez, S.R., Coats, J.S., Weldon, A.J., Calderon, M.N., Nwosu, M.C., Botimer, A.R., et al. (2016). TSLP or IL-7 provide an IL-7Rα signal that is critical for human B lymphopoiesis. Eur. J. Immunol. *46*, 2155–2161.

Mizoguchi, T., Pinho, S., Ahmed, J., Kunisaki, Y., Hanoun, M., Mendelson, A., Ono, N., Kronenberg, H.M., and Frenette, P.S. (2014). Osterix marks distinct waves of primitive and definitive stromal progenitors during bone marrow development. Dev. Cell *29*, 340–349.

Mourcin, F., Breton, C., Tellier, J., Narang, P., Chasson, L., Jorquera, A., Coles, M., Schiff, C., and Mancini, S.J. (2011). Galectin-1-expressing stromal cells constitute a specific niche for pre-BII cell development in mouse bone marrow. Blood *117*, 6552–6561.

Murshed, M., Smyth, N., Miosge, N., Karolat, J., Krieg, T., Paulsson, M., and Nischt, R. (2000). The absence of nidogen 1 does not affect murine basement membrane formation. Mol. Cell. Biol. *20*, 7007–7012.

Nakamura, Y., Arai, F., Iwasaki, H., Hosokawa, K., Kobayashi, I., Gomei, Y., Matsumoto, Y., Yoshihara, H., and Suda, T. (2010). Isolation and characterization of endosteal niche cell populations that regulate hematopoietic stem cells. Blood *116*, 1422–1432.

Omatsu, Y., Sugiyama, T., Kohara, H., Kondoh, G., Fujii, N., Kohno, K., and Nagasawa, T. (2010). The essential functions of adipo-osteogenic progenitors as the hematopoietic stem and progenitor cell niche. Immunity *33*, 387–399.

Omatsu, Y., Seike, M., Sugiyama, T., Kume, T., and Nagasawa, T. (2014). Foxc1 is a critical regulator of haematopoietic stem/progenitor cell niche formation. Nature *508*, 536–540.

Park, S.Y., Wolfram, P., Canty, K., Harley, B., Nombela-Arrieta, C., Pivarnik, G., Manis, J., Beggs, H.E., and Silberstein, L.E. (2013). Focal adhesion kinase regulates the localization and retention of pro-B cells in bone marrow microenvironments. J. Immunol. *190*, 1094–1102.

Reimand, J., Arak, T., and Vilo, J. (2011). g:Profiler–a web server for functional interpretation of gene lists (2011 update). Nucleic Acids Res. *39*, W307–W315.

Repass, J.F., Laurent, M.N., Carter, C., Reizis, B., Bedford, M.T., Cardenas, K., Narang, P., Coles, M., and Richie, E.R. (2009). IL7-hCD25 and IL7-Cre BAC transgenic mouse lines: new tools for analysis of IL-7 expressing cells. Genesis *47*, 281–287.

Revilla-I-Domingo, R., Bilic, I., Vilagos, B., Tagoh, H., Ebert, A., Tamir, I.M., Smeenk, L., Trupke, J., Sommer, A., Jaritz, M., and Busslinger, M. (2012). The B-cell identity factor Pax5 regulates distinct transcriptional programmes in early and late B lymphopoiesis. EMBO J. *31*, 3130–3146.

Reyal, F., Stransky, N., Bernard-Pierrot, I., Vincent-Salomon, A., de Rycke, Y., Elvin, P., Cassidy, A., Graham, A., Spraggon, C., Désille, Y., et al. (2005). Visualizing chromosomes as transcriptome correlation maps: evidence of chromosomal domains containing co-expressed genes–a study of 130 invasive ductal breast carcinomas. Cancer Res. *65*, 1376–1383.

Russell, S.M., Tayebi, N., Nakajima, H., Riedy, M.C., Roberts, J.L., Aman, M.J., Migone, T.S., Noguchi, M., Markert, M.L., Buckley, R.H., et al. (1995). Mutation of Jak3 in a patient with SCID: essential role of Jak3 in lymphoid development. Science *270*, 797–800.

Sugiyama, T., Kohara, H., Noda, M., and Nagasawa, T. (2006). Maintenance of the hematopoietic stem cell pool by CXCL12-CXCR4 chemokine signaling in bone marrow stromal cell niches. Immunity *25*, 977–988.

Tokoyoda, K., Egawa, T., Sugiyama, T., Choi, B.I., and Nagasawa, T. (2004). Cellular niches controlling B lymphocyte behavior within bone marrow during development. Immunity *20*, 707–718.

Tormin, A., Li, O., Brune, J.C., Walsh, S., Schütz, B., Ehinger, M., Ditzel, N., Kassem, M., and Scheding, S. (2011). CD146 expression on primary nonhematopoietic bone marrow stem cells is correlated with in situ localization. Blood *117*, 5067–5077.

Visnjic, D., Kalajzic, Z., Rowe, D.W., Katavic, V., Lorenzo, J., and Aguila, H.L. (2004). Hematopoiesis is severely altered in mice with an induced osteoblast deficiency. Blood *103*, 3258–3264.

Wang, L., Benedito, R., Bixel, M.G., Zeuschner, D., Stehling, M., Sävendahl, L., Haigh, J.J., Snippert, H., Clevers, H., Breier, G., et al. (2013). Identification of a clonally expanding haematopoietic compartment in bone marrow. EMBO J. *32*, 219–230.

Wu, J.Y., Purton, L.E., Rodda, S.J., Chen, M., Weinstein, L.S., McMahon, A.P., Scadden, D.T., and Kronenberg, H.M. (2008). Osteoblastic regulation of B lymphopoiesis is mediated by Gsalpha-dependent signaling pathways. Proc. Natl. Acad. Sci. USA *105*, 16976–16981.

Xu, C., Gao, X., Wei, Q., Nakahara, F., Zimmerman, S.E., Mar, J., and Frenette, P.S. (2018). Stem cell factor is selectively secreted by arterial endothelial cells in bone marrow. Nat. Commun. *9*, 2449.

Yi, X.Y., Wayner, E.A., Kim, Y., and Fish, A.J. (1998). Adhesion of cultured human kidney mesangial cells to native entactin: role of integrin receptors. Cell Adhes. Commun. *5*, 237–248.

Zhang, J., and Link, D.C. (2016). Targeting of mesenchymal stromal cells by Cre-recombinase transgenes commonly used to target osteoblast lineage cells. J. Bone Miner. Res. *31*, 2001–2007.

Zhu, J., Garrett, R., Jung, Y., Zhang, Y., Kim, N., Wang, J., Joe, G.J., Hexner, E., Choi, Y., Taichman, R.S., and Emerson, S.G. (2007). Osteoblasts support B-lymphocyte commitment and differentiation from hematopoietic stem cells. Blood *109*, 3706–3712.

STAR★METHODS

KEY RESOURCES TABLE

REAGENT or RESOURCE	SOURCE	IDENTIFIER
Antibodies		
Anti-Actin, α-Smooth Muscle - Cy3 antibody, Mouse monoclonal	sigma-aldrich	Cat#C6198; RRID: AB_476856
CD45R (B220) clone RA3-6B2, PE-Cy5	eBioscience	Cat#15-0452-83; RRID: AB_468756
CD45R (B220) clone RA3-6B2, APC	eBioscience	Cat# 17-0452-83; RRID: AB_469396
CD45R (B220) clone RA3-6B2, APC-eFluor 780	eBioscience	Cat# 47-0452-82; RRID: AB_1518810
CD45R (B220) clone RA3-6B2, biotin	Biolegend	Cat#103204; RRID: AB_312989
CD249 (Lγ-51) Clone BP-1, PE	BD Biosciences	Cat#553735; RRID: AB_395018
CD249 (Ly-51), Clone 6C3, biotin	BD Biosciences	Cat# 553159; RRID: AB_394671
CD249 (Lγ-51) Clone BP-1, BV786	BD Biosciences	Cat# 740882; RRID: AB_2740531
CD2 clone RM2-5, PE-Cy7	Biolegend	Cat# 100114; RRID: AB_2563092
CD3ε, clone 145-2C11, Alexa Fluor 647	Biolegend	Cat# 100322; RRID: AB_389322
CD3ε, clone 145-2C11, biotin	Biolegend	Cat# 100304; RRID: AB_312669
CD4 clone RM4-5, biotin	eBioscience	Cat#13-0042-86; RRID: AB_466331
CD8a Clone 53-6.7, APC	BD Biosciences	Cat#553035; RRID: AB_398527
CD8a Clone 53-6.7, biotin	eBioscience	Cat# 13-0081-85; RRID: AB_466347
CD11b clone M1/70, Alexa Fluor 647	Biolegend	Cat# 101218; RRID: AB_389327
CD11b clone M1/70, PE-Cy5	eBioscience	Cat# 15-0112-83; RRID: AB_468715
CD11b clone M1/70, biotin	Biolegend	Cat# 101204; RRID: AB_312787
CD11c clone N418, PE-Cy5	Biolegend	Cat# 117316; RRID: AB_493566
CD11c clone N418, Alexa Fluor 647	eBioscience	Cat# 51-0114-82; RRID: AB_469783
CD11c clone N418, biotin	eBioscience	Cat# 13-0114-85; RRID: AB_466364
CD19 clone 1D3, PE-Cy5	eBioscience	Cat# 15-0193-83; RRID: AB_657673
CD19 Clone 1D3, BV605	BD Biosciences	Cat# 563148; RRID: AB_2732057
CD19 Clone 6D5, biotin	Biolegend	Cat# 115504; RRID: AB_313639
CD23 Clone B3B4, BV711	BD Biosciences	Cat# 563987; RRID: AB_2738525
CD24 clone M1/69, PE-Cy5	eBioscience	Cat# 15-0242-82; RRID: AB_468731
CD24 clone M1/69, biotin	BD Biosciences	Cat# 553260; RRID: AB_394739
CD31 (PECAM-1) clone 390, PE-Cy7	eBioscience	Cat# 25-0311-81; RRID: AB_469615
CD43 clone S7, FITC	BD Biosciences	Cat# 553270; RRID: AB_394747
CD43 clone S7, APC	BD Biosciences	Cat# 560663; RRID: AB_1727479
CD45 clone 30-F11, PE-Cy5.5	eBioscience	Cat# 35-0451-82; RRID: AB_469718
CD45 clone H129-326	Michel Pierres, CIML, Marseille	N/A
CD48 clone HM48-1, Alexa Fluor 647	Biolegend	Cat# 103416; RRID: AB_571987
CD48 clone HM48-1, APC-Cy7	BD Biosciences	Cat# 561242; RRID: AB_10644381
CD49d (Integrin alpha 4) clone R1-2, FITC	eBioscience	Cat# 11-0492-81; RRID: AB_465082
CD51 (Integrin alpha V) clone RMV-7, PE	eBioscience	Cat# 12-0512-81; RRID: AB_465703
CD51 (Integrin alpha V) clone RMV-7, Biotin	eBioscience	Cat# 13-0512-81; RRID: AB_466476
CD54 Clone 3E2, BV421	BD Biosciences	Cat# 564704; RRID: AB_2738903
CD71 Clone C2, BV605	BD Biosciences	Cat# 563013; RRID: AB_2737950
CD105 clone MJ7/18, PE-CF594	BD Biosciences	Cat# 562762; RRID: AB_2737776
CD106 (VCAM-1) clone 429, Biotin	eBioscience	Cat# 13-1061-81; RRID: AB_466558
CD117 (c-Kit) clone 2B8, PE-Cy5	eBioscience	Cat# 15-1171-83; RRID: AB_468788
CD117 (c-Kit) clone 2B8, PE	eBioscience	Cat# 12-1171-83; RRID: AB_465814

(*Continued on next page*)

Continued

REAGENT or RESOURCE	SOURCE	IDENTIFIER
CD135 clone A2F10, PE	Biolegend	Cat# 135306; RRID: AB_1877217
CD135 clone A2F10, PE-Cy7	BD Biosciences	Cat# 562537; RRID: AB_2737639
CD127 (IL-7Rα) clone A7R34, Alexa Fluor 647	Biolegend	Cat# 135020; RRID: AB_1937209
CD150 (SLAM) clone TC15-12F12.2, PE	Biolegend	Cat# 115904; AB_313683
CD150 (SLAM) clone TC15-12F12.2, PE-Cy7	Biolegend	Cat# 115913; AB_439796
CD184 (CXCR4) clone 2B11, PE	eBioscience	Cat# 12-9991-81; RRID: AB_891393
CD317 (BST2, PDCA-1) clone eBio927, PE	eBioscience	Cat# 12-3172-81; RRID: AB_763421
Green Fluorescent Protein (GFP) Antibody	Aves	Cat# GFP-1020; RRID: AB_10000240
Ly-6G/Ly-6C (Gr1) clone RB6-8C5, APC	eBioscience	Cat# 17-5931-81; RRID: AB_469475
Ly-6G/Ly-6C (Gr1) clone RB6-8C5, PE-Cy5	eBioscience	Cat# 15-5931-81; RRID: AB_468812
Ly-6G/Ly-6C (Gr1) clone RB6-8C5, biotin	eBioscience	Cat# 13-5931-85; RRID: AB_466801
IgM Clone R6-60.2, BV421	BD Biosciences	Cat# 562595; RRID: AB_2737671
IgM Clone R6-60.2, PE-CF594	BD Biosciences	Cat# 562565; RRID: AB_2737658
Anti-Laminin antibody	abcam	Cat# ab11575; RRID: AB_298179
Mouse Leptin R, biotin	R&D	Cat# BAF497; RRID: AB_2296953
NG2 Chondroitin Sulfate Proteoglycan	Millipore	Cat# AB5320; RRID: AB_11213678
NG2 Chondroitin Sulfate Proteoglycan, Biotin	Millipore	Cat# AB5320B
NG2 Chondroitin Sulfate Proteoglycan, Alexa Fluor®488	Millipore	Cat# AB5320A4; RRID: AB_11203143
NK-1.1 Clone PK136, APC	BD Biosciences	Cat# 561117; RRID: AB_10563422
CD49b clone DX5, biotin	Biolegend	Cat# 108904; RRID: AB_313411
TEM7/PLXDC1 Antibody (197C193 (IM193))	Novus biologicals	Cat# NB100-56557; RRID: AB_838963
Ly-6A/E (Sca-1) clone D7, Alexa Fluor 700	eBioscience	Cat# 56-5981-80; AB_657837
Ly-6A/E (Sca-1) clone D7, BV421	BD Biosciences	Cat# 562729; RRID: AB_2737750
Anti-Stat5 (pY694) clone 47/Stat5(pY694), Alexa Fluor 647	BD Biosciences	Cat# 612599; RRID: AB_399882
TdT clone 19-3, FITC	Miltenyi Biotech	Cat# 130-100-687; RRID: AB_2654106
TER-119 clone TER-119, PE-Cy5	eBioscience	Cat# 15-5921-82; RRID: AB_468810
TER-119 clone TER-119, APC-eFluor 780	eBioscience	Cat# 47-5921-82; RRID: AB_1548786
TER-119 clone TER-119, biotin	Biolegend	Cat# 116204; RRID: AB_313705
Ly6D clone 49-H4, eFluor 450	eBioscience	Cat# 48-5974-80; RRID: AB_2574089
Endomucin clone V.7C7, Alexa Fluor 647	Santa Cruz Biotechnology	Cat# sc-65495 AF647; RRID: AB_2100037
Human CD34 Class II clone QBEnd 10, Unconjugated,	Agilent Dako	Cat# IR632
Human Terminal Deoxynucleotidyl Transferase clone SEN28	Leica biosystem	Cat# NCL-L-TdT-339; RRID: AB_564025
Human BST2 clone EPR5648	Abcam	Cat# ab134061
Human IL7, rabbit polyclonal	Sigma	Cat# HPA019590; RRID: AB_10794621
Human CXCL12 clone D8G6H	Cell Signaling Technology	Cat# 97958S
TEM7/PLXDC1 clone 197C193 (IM193)	Novus Biologicla	Cat# NB100-56557; RRID: AB_838963
Anticorps Nidogen (ELM1): sc-33706	Santa Cruz Biotechnology	Cat# sc-33706 AF647; RRID: AB_627519
CD31 (PECAM-1), goat polyclonal, Alexa Fluor 488	R&D systems	Cat# FAB3628G; RRID: AB_10972784
Alexa Fluor 594 AffiniPure F(ab')$_2$ Fragment Donkey Anti-Rabbit IgG (H+L)	Jackson ImmunoResearch	Cat# 711-586-152; RRID: AB_2340622
Alexa Fluor® 647 AffiniPure F(ab')$_2$ Fragment Donkey Anti-Rabbit IgG (H+L)	Jackson ImmunoResearch	Cat# 711-606-152; RRID: AB_2340625
AffiniPure F(ab')$_2$ Fragment Goat Anti-Mouse IgG (H+L)	Jackson ImmunoResearch	Cat# 115-006-003; RRID: AB_2338466
Alexa Fluor 488 AffiniPure F(ab')$_2$ Fragment Goat Anti-Mouse IgG (H+L)	Jackson ImmunoResearch	Cat# 115-546-003; RRID: AB_2338859
Alexa Fluor 647 AffiniPure F(ab')$_2$ Fragment Goat Anti-Mouse IgG (H+L)	Jackson ImmunoResearch	Cat# 115-606-003; RRID: AB_2338921

(*Continued on next page*)

Continued

REAGENT or RESOURCE	SOURCE	IDENTIFIER
Goat anti-Chicken IgY (H+L) Secondary Antibody, Alexa Fluor 488	Thermo Fisher Scientific	Cat# A-11039; RRID: AB_2534096
Donkey anti-Rat IgG (H+L) Highly Cross-Adsorbed Secondary Antibody, Alexa Fluor 594	Invitrogen	Cat# A-21209; RRID: AB_2535795
Streptavidin APC	eBioscience	Cat# 17-4317-82
Streptavidin BV480	BD Biosciences	Cat# 564876
Streptavidin PE-Texas Red	BD Biosciences	Cat# 551487; RRID: AB_10054235
Streptavidin Alexa Fluor 700	ThermoFisher	Cat# s21383
Biological Samples		
paraffin embedded adult osteo-medullary biopsies	Institut Paoli-Calmettes, Marseille, France	http://www.institutpaolicalmettes.fr/
Chemicals, Peptides, and Recombinant Proteins		
Hydroxyurea	Merk Millipore	Cat# 400046
Pierce 16% Formaldehyde (w/v), Methanol-free	Thermo Scientific	Cat# 28908
Liberase TL Research Grade	Merk	Cat# 05401020001 Roche
Collagenase from Clostridium histolyticum	Sigma	Cat# C0130
SYTOX Blue Nucleic Acid Stain	Invitrogen	Cat# S11348
Draq 7	Biolegend	Cat# 424001
LIVE/DEAD Fixable Aqua Dead Cell Stain Kit	ThermoFisher	Cat# L34957
Critical Commercial Assays		
TaqMan Universal PCR Master Mix	Applied Biosystems	Cat# 4304437
CellsDirect One-Step qRT-PCR Kit	Invitrogen	Cat# 11753500
GT 96.96 Dynamic Array Sample & Assay Loading Reagent Kit—10 IFCs	Fluidigm	Cat# 85000827
Control Line Fluid Kit—96.96	Fluidigm	Cat# 89000021
RNeasy Plus Micro Kit	QIAGEN	Cat# 74034
TO-PRO-3 Iodide (642/661)	Thermo scientific	Cat# T3605
Fixation/Permeabilization Solution Kit	BD Biosciences	Cat# 554714
PerFix EXPOSE (Phospho-Epitopes Exposure kit)	Beckman and coulter	Cat# PN B26976
C1 Single-Cell Reagent Kit for Preamp	Fluidigm	Cat# 100-5319
Endogenous Biotin-Blocking Kit	Invitrogen	Cat# E21390
1X RBC Lysis Buffer	eBioscience	Cat# 00-4333-57
CFSA Lame adhesive	Leica	Cat# 39475209
96.96 Dynamic Array IFC for Gene Expression	Fluidigm	Cat# BMK-M-96.96
C1 Single-Cell Open App IFC, 5–10 μm	Fluidigm	Cat# 100-8133
ProLong Gold Antifade Mountant	Thermo Fisher	Cat# P36934
Actb TaqMan® Gene Expression Assays	Thermo Fisher	Mm00607939_s1
Alpl TaqMan® Gene Expression Assays	Thermo Fisher	Mm00475834_m1
Angpt1 TaqMan® Gene Expression Assays	Thermo Fisher	Mm00456503_m1
Col1a1 TaqMan® Gene Expression Assays	Thermo Fisher	Mm00801666_g1
Cspg4 TaqMan® Gene Expression Assays	Thermo Fisher	Mm00507257_m1
Cxcl12 TaqMan® Gene Expression Assays	Thermo Fisher	Mm00445553_m1
Cx3cl1 TaqMan® Gene Expression Assays	Thermo Fisher	Mm00436454_m1
Eng TaqMan® Gene Expression Assays	Thermo Fisher	Mm00468256_m1
Enpep TaqMan® Gene Expression Assays	Thermo Fisher	Mm00468278_m1
Foxc1 TaqMan® Gene Expression Assays	Thermo Fisher	Mm01962704_s1
Gja1 TaqMan® Gene Expression Assays	Thermo Fisher	Mm01179639_s1
Gjc1 TaqMan® Gene Expression Assays	Thermo Fisher	Mm01253027_m1
Gapdh TaqMan® Gene Expression Assays	Thermo Fisher	Mm99999915_g1

(*Continued on next page*)

Continued

REAGENT or RESOURCE	SOURCE	IDENTIFIER
Icam1 TaqMan® Gene Expression Assays	Thermo Fisher	Mm00516024_g1
Il7 TaqMan® Gene Expression Assays	Thermo Fisher	Mm00434291_m1
Itgav TaqMan® Gene Expression Assays	Thermo Fisher	Mm00434486_m1
Jam2 TaqMan® Gene Expression Assays	Thermo Fisher	Mm00470197_m1
Kitl TaqMan® Gene Expression Assays	Thermo Fisher	Mm00442972_m1
Lama4 TaqMan® Gene Expression Assays	Thermo Fisher	Mm01193660_m1
Lepr TaqMan® Gene Expression Assays	Thermo Fisher	Mm00440181_m1
Nid1 TaqMan® Gene Expression Assays	Thermo Fisher	Mm00477827_m1
Prrx1 TaqMan® Gene Expression Assays	Thermo Fisher	Mm00440932_m1
Pdgfra TaqMan® Gene Expression Assays	Thermo Fisher	Mm00440701_m1
Runx2 TaqMan® Gene Expression Assays	Thermo Fisher	Mm00501584_m1
Vcam1 TaqMan® Gene Expression Assays	Thermo Fisher	Mm01320970_m1
Deposited Data		
Affimetrix Microarray datasets	This paper	GEO: GSE90588
Affimetrix Microarray datasets	Ding et al., 2012	GEO: GSE33158
Affimetrix Microarray datasets	Greenbaum et al., 2013	GEO: GSE43613
Affimetrix Microarray datasets	https://www.ncbi.nlm.nih.gov/geo/	GEO: GSE66206
Affimetrix Microarray datasets	Nakamura et al., 2010	GEO: GSE17597
Affimetrix Microarray datasets	http://www.immgen.org	GEO: GSE15907
Affimetrix Microarray datasets	Lee et al., 2018	GEO: GSE114469
Affimetrix Microarray datasets	Decker et al., 2017	GEO: GSE84387
Affimetrix Microarray datasets	Méndez-Ferrer et al., 2010	GEO: GSE55802
Affimetrix Microarray datasets	James et al., 2015	ArrayExpress: A-GEOD-11339
single cell RNaseq datasets	This paper	GEO: GSE121568
Experimental Models: Organisms/Strains		
Mouse: IL7-Cre	Repass et al., 2009	N/A
Mouse: C57BL/6J Gt(ROSA)$^{26Sortm1(EYFP)Cos}$/J	The Jackson Laboratory	JAX: 006148
Mouse: Nid1^{Tm1Ron}	Murshed et al., 2000	N/A
Mouse: C57BL/6JRj	Janvier labs	N/A
Mouse: C57BL/6NRj	Janvier labs	N/A
Software and algorithms		
DIVA version 8.01	BD Biosciences	http://www.bdbiosciences.com/
FlowJo version 10	TreeStar	https://www.flowjo.com/
Fiji version 1.52 g	ImageJ	https://fiji.sc/
MATLAB version 9	MathWorks	https://www.mathworks.com/
R studio version 8	Rstudio	https://www.rstudio.com/
Prism version 5	GraphPad	https://www.graphpad.com/

CONTACT FOR REAGENT AND RESOURCE SHARING

Further information and requests for resources and reagents should be directed to and will be fulfilled by the Lead Contact, Stéphane J.C. Mancini (stephane.mancini@inserm.fr).

EXPERIMENTAL MODEL AND SUBJECT DETAILS

Mice

C57BL/6J and C57NL/6N mice were purchased from Janvier Laboratories, France. IL7cre Rosa26-eYFP (Repass et al., 2009) were backcrossed for more than eight generations onto a C57BL/6J background. *Nid1*$^{-/-}$ mice (Murshed et al., 2000) backcrossed on a C57BL/6N background were a kind gift from Pr. Krieg (University of Cologne). Both male and female mice were used between

6 and 15 weeks of age and were housed under specific pathogen-free conditions. Animals were randomly included in the experiments according to genotyping results. The numbers of mice used per experiment are stated in the figure legends. Mice were handled in accordance with the French Guidelines for animal handling (Agreement #02294.01) and the EU Directive 2010/63/EU.

For the generation of bone marrow chimeras, recipient mice were lethally irradiated with 7 Gy of total body irradiation (X-ray source, RS-2000 irradiator) one day before transplantation. Amoxicilline was added to the drinking water at 0.25 mg/ml and left during 2 weeks. Transplantation of $5x10^6$ donor bone marrow cells was performed by intra venous injection via the retro-orbital sinus. BM B cell development was analyzed 15 week post transplantation.

Hydroxyurea treatments were performed by injecting intraperitoneally 1 mg/g of body weight at a rate of 2 injections separated by 7 hours per day for 2 days as previously described (Espeli et al., 2009). BM B cell development was analyzed 7 days post injection.

Human tissues

Osteo-medullary biopsies from four normal male and female adult subjects from 18 to 56 years old were used. Patients provided informed consent in line with the Declaration of Helsinki before sample collection. The study protocol was approved by the institutional review board at Institut Paoli-Calmettes (agreement #IPC 2018-002).

METHOD DETAILS

Flow cytometry and cell sorting

For flow cytometry experiments, single-cell suspensions were stained using standard protocols and the antibodies listed in Supplemental Experimental Procedures. Dead cells were excluded using Sytox Blue, LIVE/DEAD® Fixable Aqua Dead Cell Stain (ThermoFisher) or DRAQ7 (Beckman Coulter).

To analyze hematopoietic cell populations, BM cells were extracted, lysed (1X RBC lysis buffer, eBiosciences) and stained. Cell-cycle analysis was performed by staining double-stranded nucleic acids with TO-PRO-3 (ThermoFisher Scientific) following fixation and permeabilization of the cells using the Cytofix/Cytoperm kit (BD Biosciences). Phosphorylated STAT5 was detected using the anti-phosphoprotein pSTAT5 antibody following fixation and permeabilization of the cells with the PerFix EXPOSE kit (Beckman Coulter). The lineage cocktail (Lin) used to identify the hematopoietic progenitors contains the following markers: CD3, CD4, CD8α, DX5, B220, CD19, CD11b, CD11c, Gr1 and Ter119. Hematopoietic subsets were defined as follow: LT-HSC: $Lin^-Sca1^+CD11^+$(LSK)$CD150^+CD48^-CD135^-$; ST-HSC: LSK $CD150^-CD48^-CD135^-$; MPP2: LSK $CD150^+CD48^+CD135^-$; MPP3: LSK $CD150^-CD48^+CD135^-$; MPP4: LSK $CD150^-CD135^+$; Myeloid progenitors: $Lin^-CD117^+Sca1^-$; CLP: $Lin^-CD117^{lo}CD127^+CD135^+$; pre-pro-B: $B220^+CD19^-CD43^+CD24^-CD117^+CD127^+$; pro-B: $CD19^+B220^+IgM^-CD23^-BP1^-CD2^-CD117^+$; pre-BI: $CD19^+B220^+IgM^-CD23^-BP1^+CD2^-CD117^+$; pre-BII: $CD19^+B220^+IgM^-CD23^-CD2^+$; Immature B cells: $CD19^+B220^+IgM^+CD23^-$; Recirculating B cells: $CD19^+B220^+IgM^+CD23^+$.

For analysis of BM stromal cells, femur and tibia from mice were crushed, deposited on a 100μm cell strainer and rinsed three times with PBS to recover cells from the conduit fraction in the eluate. Mesenchymal and endothelial cells associated to the sub-endosteal region were recovered from the crushed bones. Conduit fractions were incubated with 0.1mg/mL of Liberase TL Research Grade (Roche) and 10 U/mL DNaseI (Invitrogen) at 37°C for 20 minutes. The bone fraction was treated with 2 mg/ml collagenase I and 10 U/mL DNaseI at 37°C for 40 minutes. BM stromal cells were enriched by negative selection using immunomagnetic anti–rat IgG Dynabeads (Invitrogen) and antibodies recognizing CD45 (H129–326 supernatant), Ter-119 (BD Biosciences) and B220 (eBioscience). The stroma lineage cocktail is composed of the following markers: B220, CD19, CD11b, CD11c, Gr1, Ter119 and CD117. For transcriptomic analysis, $CD54^+BP1^+$ stromal cells were sorted from WT mice, and $CD54^+BP1^+YFP^+$ and $CD54^+BP1^+YFP^-$ cells were sorted from IL7-Cre/Rosa-eYFP mice. $CD31^+$ $Sca1^{low}$ sinusoidal BMEC were sorted from WT mice. FACS analysis was performed on a FACS LSRII and cell sorting on a FACSAria III (BD Biosciences). Data were analyzed using DiVa Version 8.01 (BD Biosciences) or FlowJo Version 10 software (TreeStar).

Immunohistofluorescence

Femurs and tibias were incubated for four hours in PFA 4% prepared in PBS, decalcified and incubated in cryoprotective buffer as previously described (Kusumbe et al., 2015). Bones embedded in OCT were cryosectioned on Superfrost+ slides and immediately fixed in acetone for 5 min at −20°C. After drying, sections were rehydrated in PBS for 5 min, saturated in blocking solution (Purified Goat anti-mouse, Jackson ImmunoResearch, BSA 5%, Saponin 0.05% in PBS) for 30 min and finally incubated with primary antibodies in a humidified chamber overnight at 4°C or for 1 h at room temperature. After washing three times, slides were incubated with the appropriate secondary antibodies for 1 h at room temperature and mounted with Prolong (Pierce). Images were acquired in z on 10 to 15μm for 3D reconstruction using LSM780 or LSM880 confocal microscopes (Carl Zeiss) and processed in Fiji (https://fiji.sc/).

Quantification of confocal images

Custom MATLAB scripts were developed for calculation of the 3D distance between pro-B and nearest $LepR^+$ cells, $LepR^+Nid^+$ cells, $Nid1^{hi}$ arteries and bone surface. LepR and Nidogen images were segmented by successively median filtering over 3 by 3 pixels, optimized thresholding and erosion, dilatation over 1 pixel. Finally, objects smaller than 70 voxels (128.7 μm3) were discarded

from the final segmented result (binary images). Double positive structures, $LepR^{+}Nid^{+}$, were defined as pixels segmented both for LepR and for Nidogen. Arteries were detected using a higher threshold coefficient, and by discarding objects smaller than 1 000 voxels (1 838 μm3). To get the envelope of the entire tissue, DAPI filtering was performed over 5 by 5 pixels and erosion, dilatation over 12 pixels, to ultimately keep the convex shape surrounding the largest segmented object. MATLAB codes used to calculate threshold values, freely obtained from the MATLAB file-exchange website, were written by Martín D., based on the work of Tsai W. for LepR staining (optimal threshold), and by Marti, F.T. for Nidogen and DAPI staining (moment threshold).

For each 3D image stack, pro-B cells were manually identified by TdT staining on the maximum projection of each stack using the ImageJ cell count plugin. Their axial position was then defined as corresponding to the maximum fluorescence intensity along z, for each x, y position. Since the TdT staining can be more or less diffuse from cell to cell, the fluorescence intensity was averaged in each plane over 3 by 3 pixels around the detected position. For control, random positions were generated, with a number equal to the number of pro-B cells detected in each stack. A mask was created in 3D to allow selecting these random positions. This mask was defined by delineating the entire tissue, using the convex envelope surrounding all DAPI-stained cells. The LepR segmented image stack was removed from this mask to allow cells to be positioned only in the parenchyma. This mask was dilated by 4 μm, corresponding to the average cell radius, to avoid random cells overlapping the sinusoids. A random set of pixel positions was selected within the mask to allow comparison between real and randomized cells.

3D Euclidian distances from each segmented staining were computed over the whole image stack using bwdistsc1. This MATLAB function provides the distance from any point to the segmented structure and allowed to accommodate for anisotropic calibrations: 1.1 μm in x, y and 1.5 μm in z. The distance was then assessed for the 3D position of each real pro-B and randomly positioned cells. Since bone sections were cut along the x axis, the distance from the bone border was computed along the orthogonal, y axis, from each position of each real pro-B and randomly positioned cells to the border of the mask created from the convex DAPI staining.

Immunohistochemistry

Osteo-medullary biopsies were formalin-fixed and decalcified in 0.27 M Ethylene diamine tetra acetic acid (EDTA) before embedding in paraffin. 1.5 to 3 μm sections were used. Immunohistochemistry was performed on a Ventana Discovery XT biomarker platform. Staining with the anti-CD34 (QBEnd-10, Beckman Coulter) and anti-TdT (Sen28, Novocastra) antibodies was performed after antigen retrieval at pH 8. Staining with the anti-CD317 (ab134061, Abcam), anti-IL7 (HPA019590, Sigma Aldrich), anti-CXCL12 (D8G6H, Cell Signaling Technology) and anti-PLXDC1 (197C193, Novus Biologicals) antibodies was performed after antigen retrieval at pH 6. Multiplex staining was performed using the Discovery purple kit (Ventana), together with DAB substrate or the Discovery yellow kit (Ventana). Slides were counterstained with hematoxylin.

Gene expression profiling

qPCR analysis

Single cells were sorted in two separate experiments using the autoclone module on an AriaIII sorter (Becton Dickinson) directly into C1 chips (Fluidigm). Single cell loading, cell lysis and the pre-amplification steps using Taqman primers (see Supplemental Experimental Procedures) were performed using the C1 auto-prep system according to the manufacturer's instructions (Fluidigm). Pre-amplified products were diluted in 25 μL of C1 DNA dilution reagents before further processing using Biomark (Fluidigm). Bulk stromal cells were directly sorted into 96-well plates containing Cells Direct Reaction Mix (Life Technologies) using the autoclone module on an AriaIII sorter (Becton Dickinson). Each subpopulation analyzed was obtained from two independent sorting processes. Cell lysis and pre-amplification with Taqman primers (22 Cycles) were performed according to the Fluidigm Advanced Development Protocol. Transcript quantization in single or bulk sorted cells was performed using microfluidic real-time PCR on Dynamic Array IFCs (Biomark, 96.96 Dynamic Arrays, Fluidigm). Ct values were calculated using the system's software (BioMark Real-time PCR Analysis; Fluidigm) and filtered based on expression levels for GAPDH and expression of the surface cell markers used for the cell sorting. Gene expression analysis was performed with heatmaps generated using Morpheus (Broad institute). Unsupervised hierarchical clustering was performed using one minus Pearson's correlation distance metrics and the average linkage method.

Single cell RNaseq analysis

CD54+BP1+ PSS cells, CD51+BP1- mesenchymal cells and CD31+ BMEC were sorted by flow cytometry and mixed together. They were then subjected to the 10X Genomics Chromium Single-Cell 3′ v2 protocol according to the manufacturer's instructions by HalioDX (Marseille, France), and the resulting libraries were sequenced on an Illumina NextSeq500. A second replicate was performed in the same conditions. Both datasets are available in the GEO database (GEO: GSE121568).

Cell Ranger software v2.1.1 was used to processes FASTQ raw files: reads alignment to the mm10 genomes, filtering, barcode counting and unique molecular identifier (UMI) counting. Cells outside 2 medians absolute deviation (MADs) from the median for UMI log-counts and 3 MADs from the median for log-transformed number of genes detected were excluded, as well as cells above 5 MADs from the median for the percentage of mitochondrial genes. Genes not expressed in any cells of the remaining cells were removed. Unsupervised clustering of single-cell RNA-seq 10X Chromium data and t-distributed stochastic neighbor embedding (tSNE) for 875 cells with expression detected for 15,872 genes were performed with the Seurat package (v2.3.4) in R as described previously (Macosko et al., 2015). Gene expression measurements were normalized for each cell by the total expression, multiplied by a scale factor of 10,000 and log transformed. Variable genes were identified with the FindVariableGenes function of Seurat. Cell to cell variation driven by the number of detected molecules as well as the percentage of mitochondrial genes were regressed with the

ScaleData function. A principal component analysis (PCA) was then performed on variable genes and revealed that the first 11 principal components (PCs) were significant with the jackstraw procedure (Macosko et al., 2015) and by identifying in the graph the elbow of the standard deviation of PCs. These 11 PCs were then used to cluster the cells using the Louvain algorithm with the function FindClusters with the resolution parameters set to 0.6 (k parameter set to 30 for the construction of the K-nearest neighbor graph). 7 clusters were obtained, among which 2 clusters of contaminant hematopoietic cells identified with specific markers (*Ptprc, Cd69, Fcer1a, Ccl3, Ccl4* and *Cxcr4*) expressed by at least one these clusters but not by the others. The cells of these clusters were removed and the remaining cells were re-analyzed using the same procedure from normalization to clustering. This time the first 7 PCs of PCA were found to be significant. Unsupervised clustering of the cells on the 7 PCs with the same parameters as before resulted in 6 clusters. Positive and negative markers for each cluster were determined with the function FindAllMarkers of the Seurat package using the default Wilcoxon rank sum test and Bonferroni p values correction for multiple testing. Finally a tSNE were run on the 7 PCs using the RunTSNE function of Seurat with default parameters except the do.fast option set to true. Number of cells analyzed: PSS cells, n = 271; L-type BMEC, n = 163; H-type BMEC, n = 137; OB, n = 86; Pericytes, n = 54; MSC, n = 18.

Microarray analysis

Stromal cells were directly sorted in RLT Buffer for mRNA purification using an RNeasy plus micro-kit (QIAGEN). mRNA quality was evaluated using an Agilent 2100 (Pico Chip) before sending samples to the GenomEast Platform (http://genomeast.igbmc.fr/; Strasbourg, France). Affymetrix MoGene 1.0 ST and 430 2.0 raw CEL files, either obtained from in-house experiments or downloaded from the Gene Expression Omnibus (GEO) public database (see Supplemental Experimental Pocedures) were processed and normalized by applying the Robust Multichip Average (RMA) method, using the Oligo package through Bioconductor in the R statistical environment (version 3.2.0).

Quality-control for array hybridization and compatibility between the different sources was also assessed using Oligo. To do so, boxplots and density plots of raw and RMA-normalized expression data and subsequent classification analyses were examined. Probe sets for which the normalized expression value was less than 6 (log2 scale) across all arrays were considered as not expressed, and were therefore removed from the analysis. PCA was performed on the samples using the MultiExperiment Viewer (MeV version 4.8.1) on Probesets that showed a minimal 2-fold differential expression (in linear scale) between at least two cell populations. Heatmaps were generated using Morpheus software. Unsupervised hierarchical clustering was performed using one minus Pearson's correlation distance metrics and the average linkage method.

The human and mouse stromal cell datasets were aggregated as previously described (Charbord et al., 2014). Probes with multiple matching sequences were removed using version 17 of the custom ChIP definition file (Dai et al., 2005). PCA analysis was performed either on the 14437 genes found in common between the datasets or on the genes found in the interactome between PSS cells and LT-HSC, pre-pro-B or pro-B cells.Affymetrix datasets generated in the course of this study were uploaded to the GEO database under accession number GEO: GSE90588.

Interactome analysis

The bioinformatics pipeline can be split into four main steps: collection of interaction data, building interactome reference map, normalization of microarray data with conversion of gene identifiers conversions, and comparison of genes present in the different cellular populations.

Interactome reference map

Interactome integration and analysis was done with tools initially developed for Interactome-Transcriptome analysis (Garcia et al., 2014). For the interactome analysis, several protein-protein interaction (PPI) databases were downloaded, parsed and integrated by superimposing all the interactions found. PPIs from the Database of Interacting Proteins, Human Protein Reference Database, IntAct, the Molecular INTeraction database were integrated to build the interactome. A total of 13202 genes and 70530 interactions were mapped in the interactome. Protein identifiers were mapped to Entrez GeneID accession numbers using correspondence tables downloaded from the NCBI FTP site (date: November 5th, 2014; ftp://ftp.ncbi.nlm.nih.gov/gene/DATA/gene_info.gz). In addition to the cells profiled in-house, publicly available datasets were downloaded from the GEO as raw CEL files. All datasets studied were analyzed on the Affymetrix Mouse Gene 1.0 ST platform data. Microarray data were parsed, underwent quality-control and renormalized using the R/Bioconductor (Oligo package) and the RMA algorithm. Probes were then mapped to Entrez Gene identifiers by maximum median value (Reyal et al., 2005). To compare gene expression from multiple samples, genes were classed as expressed/not expressed for each sample using the postprocessing approach described for the Immgen dataset (Heng and Painter, 2008). Briefly, gene expression data was modeled by applying a Gaussian mixture distribution (the number of chosen Gaussians was k = 4) (Package R Nor1Mix). The first Gaussians modeled were considered non-expressed genes. The threshold was set to 95% for the second Gaussian.

Gene accession number conversion

To compare gene expression profiles for mouse cell populations using a human interactome reference map, gene IDs had to be homogenized. *Mus musculus* Entrez GeneID accession numbers were automatically converted to *Homo sapiens* accession numbers using the NCBI Homologene database downloaded as a flat file from the NCBI FTP site (ftp://ftp.ncbi.nih.gov/pub/HomoloGene/). The final conversion to gene symbols was performed using the gene_info.gz file from the NCBI FTP site (ftp://ftp.ncbi.nlm.nih.gov/gene/DATA/gene_info.gz).

GO filtering

To focus on genes coding for surface or extracellular proteins, GO annotation-based filtering was performed on the genes from the mouse genome. The GO terms selected for this filtering were: GO:0009897, GO:0005887, GO:0030246, GO:0031012, GO:0005581, GO:0005923, GO:0048535, GO:0030595 and GO:0008083.

Population comparison

Interactions between $YFP^+CD54^+BP1^+$ stromal cells from IL7-Cre/Rosa-eYFP mice and LT-HSC, ST-HSC, pre-pro-B, pro-B or pre-B cells were identified using the human interactome described above. *Cis* interactions were considered to be false positives, and thus only trans interactions were considered. Trans-homotypic interactions were included in the analysis. The relevance of the genes identified in the interactome for LT and ST-HSC was further improved by crossing data from two different datasets and considering only genes identified in both (Table S2). The gene expression signatures obtained for each hematopoietic subset were compared as follow: LT-HSC versus ST-HSC, pre-pro-B versus pre-B and pro-B versus pre-B. For the comparisons, Venn diagrams were generated, assuming that genes were specific for a population when the expression level was at least 2-fold higher.

GO enrichment

GO enrichment was analyzed for each population by hypergeometric testing associated with the custom multiple testing correction procedure g:SCS implemented in gProfiler R version (Reimand et al., 2011). The threshold for significance was set to 5%, and the reference annotation set was the same size as the annotated domain.

Gene set enrichment analysis

The GSEA method from the Broad Institute was used to statistically test whether the stromal cell interactome was enriched within $CD54^+BP1^+$ stromal cells, sBMEC and osteoblasts ($Alcam^-Sca1^-$ or $Alcam^+Sca1^-$) compared to each other. The stromal cell interactome GeneSet was added to the c2v5.1 public GeneSet collection (4726 GeneSets) from the Molecular Signatures Database (MSigDB) [Subramanian, Tamayo et al. (2005, PNAS 102, 15545-15550)] to provide the adequate statistical power. Statistical analysis was performed by determining the false discovery rate (q-value) based on 1,000 random permutations between all the GeneSets. Results were considered significant when the FDR q-value was below 0.25, as recommended by the software developers.

QUANTIFICATION AND STATISTICAL ANALYSIS

The number of biological replicates is indicated in the relevant figure legends. Error bars for pooled replicates represent standard error of the mean (SEM). The distribution of samples was determined by applying the Kolmogorov-Smirnov test. Samples were compared using a two-tailed unpaired t test or a Mann-Whitney test when normality was not reached. All statistical analyses were performed with GraphPad Prism 6. *, $p < 0.05$; **, $p < 0.01$; ***, $p < 0.001$.

DATA AND SOFTWARE AVAILABILITY

The accession numbers for the microarray and single cell RNAseq datasets reported in this paper are GEO: GSE90588 and GEO: GSE121568 respectively.